Transition Metal-Assisted Growth of Graphene and Thin-Layer Graphite (Few-layer Graphene) Films and their Characterisation

A thesis submitted towards partial fulfilment of
BS-MS Dual Degree Programme

by

Jensheer S S

(Reg No: **20111031**)

Under the guidance of

Prof. Rodney S. Ruoff

Director of CMCM, UNIST

Certificate

This is to certify that this dissertation entitled "Transition Metal-Assisted Growth of Graphene and Thin Layer Graphite (Few-layer graphene) Films, their Characterisation" towards the partial fulfilment of the BS-MS dual degree programme at the Indian Institute of Science Education and Research, Pune represents original research carried out by **Jensheer S S** at Ulsan National Institute of Science and Technology (UNIST) under the supervision of **Prof. Rodney S. Ruoff**, Director, Center for Multidimensional Carbon Materials (CMCM), Institute for Basic Science, UNIST Distinguished Professor, Department of Chemistry and School of Materials Science, UNIST, South Korea" during the academic year 2015-2016.

Signature of the Supervisor

(Prof. Rodney S. Ruoff)

March 7, 2016

Date:

Declaration

I hereby declare that the matter embodied in the report entitled "**Transition Metal-Assisted Growth of Graphene and Thin Layer Graphite (Few-layer graphene) Films and their Characterisation**" are the results of the investigations carried out by me at the Department of Chemistry and School of Materials Science, Ulsan National Institute of Science and Technology (UNIST), under the supervision of **Prof. Rodney S. Ruoff** and the same have not been submitted elsewhere for any other degree.

Jensheer S S

Date: 25-04-2016

Acknowledgement

I am deeply thankful to my supervisor, Prof. Rodney S. Ruoff, for introducing me to the exciting field of carbon materials and giving me an opportunity to do my MS thesis under his esteemed supervision. His sheer perseverance, wealth of research experience and deep commitment in the field of carbon materials has indeed influenced me a lot and gave a new dimension in scientific research. His continuous support and guidance throughput my research period was very valuable.

I am very much grateful to my co-advisor Prof. Satishchandra B. Ogale, with whom I started pursuing materials research. His expertise in material science has taught me great lessons and helped a lot in rational and critical thinking. His true dedication towards science, innovative thinking, and motivational words have always been very inspiring and helped me to work hard and sincerely.

I would like to express my sincere gratitude to my senior post-doctoral guide, Dr. Mandakini Biswal for her immense support and guidance throughout my project. She has always been a true inspiration for me and I imbibed all good qualities from her like hard work, dedication etc. which are vital for success. I deeply thank her for uplifting my research abilities, being a good mentor, giving critical comments and help preparing this dissertation. I am also grateful to Dr. Sunghwan Jin for providing the right metal foil for graphite growth, Dr. Manav Saxena and Ming Huang (graduate student) for helping me with some important characterisation techniques.

I am grateful to Institute for Basic Sciences (IBS), South Korea for supporting me with funding to carryout Master's project and to the DST inspire fellowship for my undergraduate education.

Besides, I would also like to thank all my friends, my lab mates (post- docs, graduate and undergraduate students) for creating a conducive research atmosphere and help making this journey enjoyable.

Last but not the least, I would like to thank all my beloved family members for believing in me and fulfilling all my needs throughout my life, without which I could not have achieved anything in life.

Abstract

Graphene and few layer graphene (thin-layer graphite) are important materials for a variety of potential applications. Large scale growth of these materials is an area of growing interest and is proven to be challenging. Transition metal assisted growth of graphene and thin-layer graphite by CVD (chemical vapor deposition) is one of the promising approaches presently available for a large scale growth.

This project aimed at growing monolayer and bilayer graphene (particularly in their AB-stacked form) on commercially available transition metal and alloy catalysts (Cu and CuNi) by CVD and their transfer on a dielectric substrate using various transfer methods (such as polymer-assisted wet transfer or electrochemical 'bubbling' transfer). Transferred films were analysed by methods including optical microscopy, Raman spectroscopy, SEM, AFM, and XPS.

We explored growing thin-layer graphite (what might be also called few layer graphene, particularly when in the AB-stacked configuration) on homemade mono crystalline Ni (111) foil using graphitizable precursors. Phenolic resin showed promising results. Thermogravimetric analysis (TGA) was used to study the degradation of phenolic resin along with Raman, SEM, AFM and XPS measurements.

We also aimed to grow large area graphene/thin-layer graphite on various substrates using mechanically exfoliated graphite as a seed. As-grown films were characterised by optical images, Raman spectroscopy, and SEM.

Contents

Chapter 1

Introduction

1.1 Introduction and Motivation

Carbon-based materials play a significant role in science and technology. Among which graphene and thin-layer graphite have aroused great interest, owing to electronic, optoelectronic, mechanical, barrier, and optical properties, among others.[1] Though graphene's structure has been sought since the early 1950's,[2] it did not cause much impact until it was isolated on an insulating substrate in 2004. Since then, it has been of interest for research, and led to various applications. Figure 1.1 describes important milestones in the preparation, isolation, and characterization of graphene.

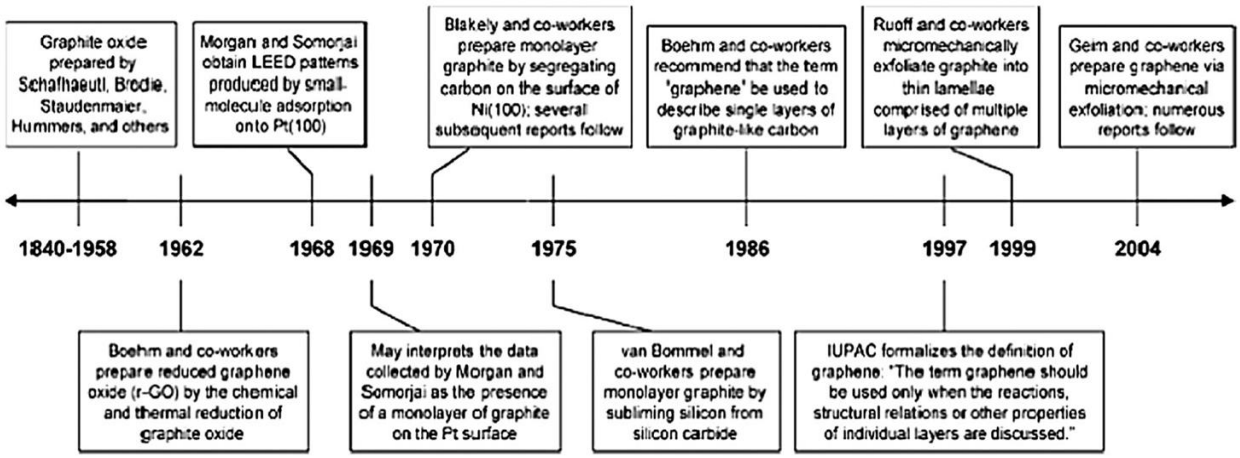

Figure 1.1: Timeline of important events in the history of the preparation, isolation, and characterization of graphene.[3]

Graphene's structure is a 2D hexagonal carbon lattice. It (as has been suggested by some authors) could be considered the basic structural element for other carbon allotropes such as fullerenes, carbon nanotubes and graphite (Figure 1.2). Its properties are intriguing and are explored in many different ways. Single-layer

graphene is a mechanically stable material and is also electrically conductive. The pure form of carbon, graphite, is many layers of graphene stacked on top of each other, the distance between in-plane carbon atoms in graphite is 0.1421 nm (sp^2 hybridization) and the in-plane bonding energy is 430 kJ/ mol, which is greater than that of diamond. The overlapping p-orbitals are filled with delocalized electrons and they form weak π-bonds. Each layer of graphite is bound by Van der Waals forces with a distance of 0.354 nm between the planes. The layered structure gives extreme anisotropy in graphite's physical properties. The weak force between the layers of graphite allows the layers to slide and gives graphite its lubrication properties which are commonly used in industrial and private applications (locks).[4] Graphite is also being employed as an electrode material in batteries, and is used in fuel cells, drawing and writing tools, in sports etc…

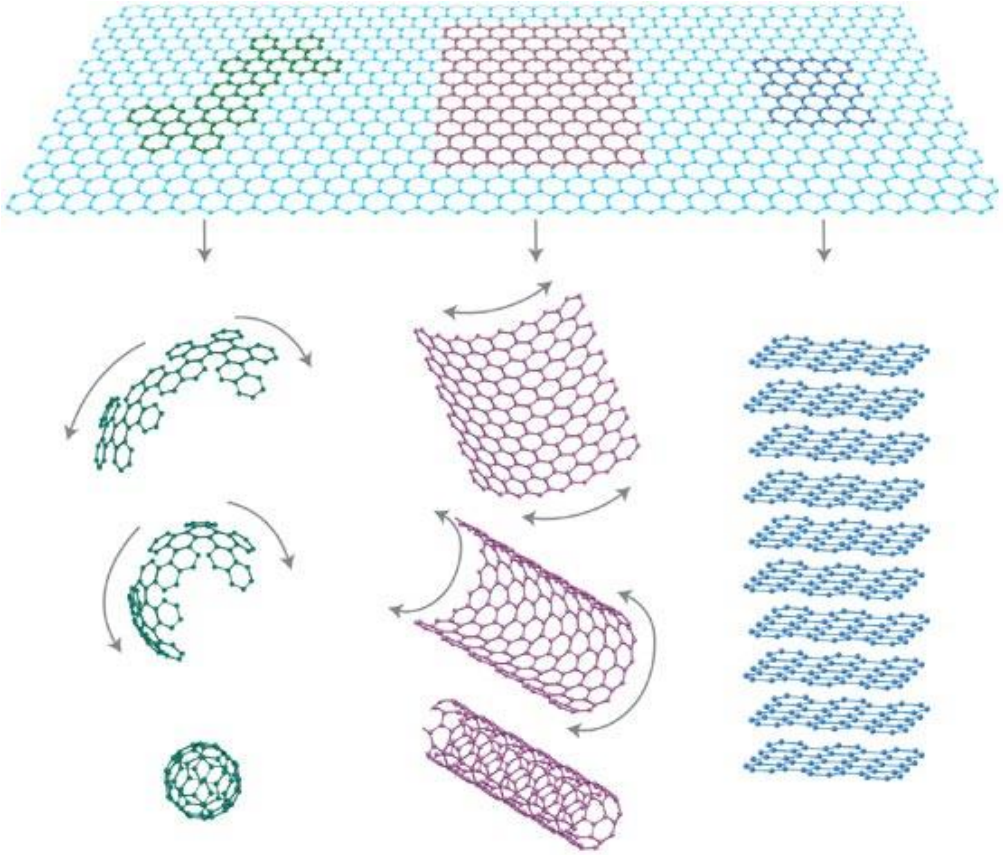

Figure 1.2: C60 fullerenes, carbon nanotubes, and graphite, all of these share the common hexagonal structure of graphene.[5]

With promising electronic properties, large-area continuous graphene film has wide application prospects in various fields, which include nanoelectronic devices, transparent conductive film, solar cell electrode, gas sensor, thin film electronic devices, among others. Graphene can be obtained from micromechanical exfoliation, chemical vapour deposition (CVD), epitaxial growth using SiC and from solution based methods (by reduction of graphite oxide).[1] Very high quality of graphene sheets with superior properties can be obtained from micromechanical exfoliation of Kish graphite or highly oriented pyrolytic graphite (HOPG).[1] However, their large scale production is limited due to small size samples. Graphene oxide can be converted to reduced graphene oxide by various reducing agents[6,7,8], but structural defects formed during the oxidation and reduction processes lead to its poor quality. Among all these methods, CVD growth and epitaxial growth from SiC have been used to produce graphene in wafer scale. However epitaxial growth on SiC substrate has certain drawbacks such as complications in the substrate preparation and difficulty in the transfer of graphene to other substrates etc.[9] The breakthrough discovery on large area high quality single-layer graphene growth on Cu foil (catalyst) using CVD by Li. *et al*, it opened up a new way for synthesising uniform large area high quality graphene on metal substrate.[10] By following CVD method, Wang et al. has achieved centimetre sized single crystals of graphene on Cu foil.[11] Nevertheless, CVD for achieving large area single crystals of bilayer and multi-layer graphene involves challenges. The non-uniformity in layer numbers, small grain size, and poor stacking are attributed to the poor quality of bilayer and multi-layer graphene. The exciting electronic properties of graphene is dependent on the way the graphene layers are stacked or arranged. Hence, there's plenty of room for studying the growth optimization there by achieving large area high quality multi-layer graphene.

The challenges associated with the growth of high quality graphene/graphite was the true motivation behind this project. My research is aimed at optimizing the growth conditions for the synthesis of these materials on various catalytic substrates using different carbon precursors. Synthesis of graphite can be achieved from various carbon precursors (coal, petroleum, natural and synthetic organic materials) at elevated temperatures (2000-3000°C). Figure 1.3 depicts the reaction scheme for carbonization and graphitization. High temperature treatment is necessary for carbon atoms to acquire enough mobility to properly pack together and rearrange well into the crystalline lattice of graphite. The individual grain size is usually in the range of

10-20 µm in these types of synthetic graphites.[4] Hence synthesis of graphite with large grain size and controlled layer numbers is still a bottleneck.

We explored the possibility of using catalytic substrates such as transition metals to reduce the temperature of graphitization. Formation of few-layer graphene via heterogeneous catalysis on various transition metal surfaces has been known for about 50 years.[12] Metal catalysts are reported to provide low activation energy pathways for the reaction to take place through the formation of intermediate compounds or by changing the oxidation states.[12] We aimed at synthesizing large area multi-layer graphene/graphite on transition metal surfaces from different carbon precursors through high temperature annealing. Noda and Inakaki reported that it is not just the high temperature treatment but an ambient gas phase has a relatively large effect on the graphitization of carbon.[13]

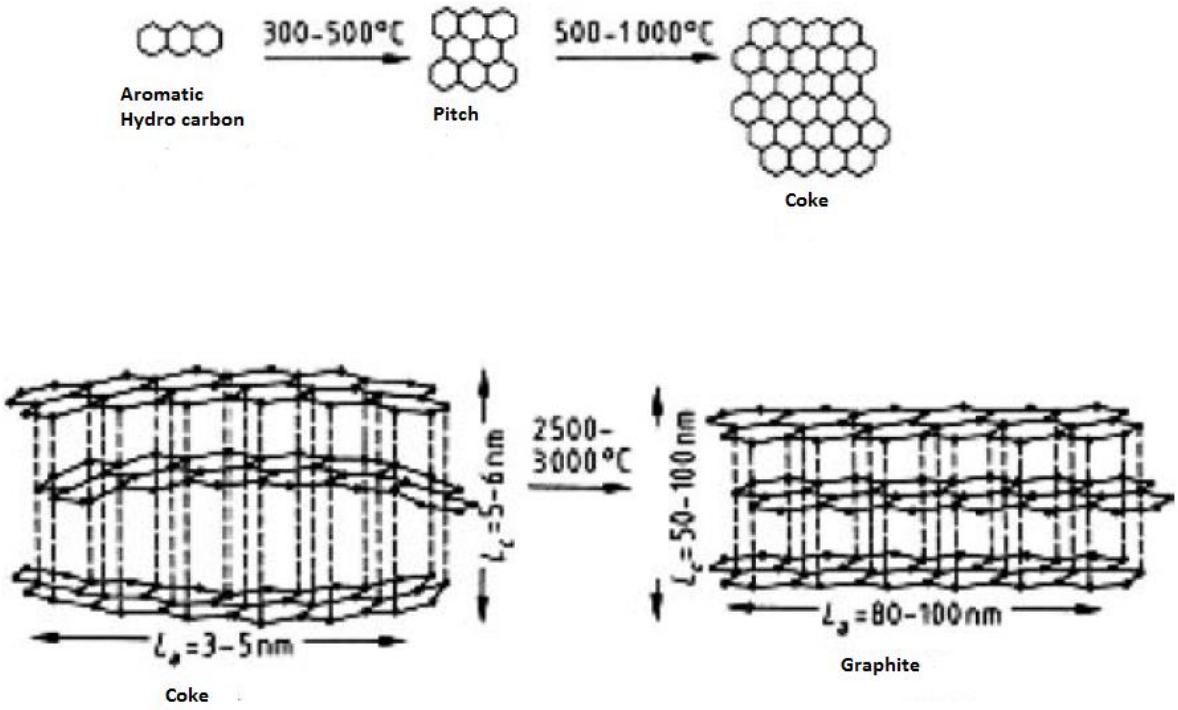

Figure 1.3: Reaction scheme for carbonization and graphitization [4].

Apart from this, we have explored the growth of single-layer and bi-layer graphene on transition metal surfaces through CVD growth optimization. This has helped us in understanding the CVD growth process in detail.

1.2 Growth of graphene/thin layer graphite on transition metals

From all discussions, it's clear that out of several methods available for synthesising large area graphene on metal surface, chemical vapour deposition is the most reliable method.

In general, CVD growth of graphene is a two-step process. The first step is the incorporation (dissolution) of carbon atoms on a metal surface followed by precipitation/segregation to yield graphene layer(s). In other words, this essentially involves the activation of the reagent gas molecule(s) and their chemical reaction that results in the deposition of film on the substrate. Blakely's group has reported that the formation of graphene on Ni surface is via precipitation/segregation.[14] But processes of segregation and precipitation are slightly different. Segregation is a process, where compositional heterogeneity is achieved at thermal equilibrium under conditions which correspond to one-phase field, while precipitation refers to in-homogeneities which arise due to equilibrium phase separation.[15] The growth of graphene on metals dependent on the solubility of carbon in these metals. Table1.1 shows a list of transition metals and their solubility values with carbon. From this table, it's clear that the highest carbon solubility is observed for Co and Ni whereas Cu has a very low carbon solubility. In high carbon soluble metals such as Ni, graphene growth is driven by chemisorption, whereas physisorption mainly determines the carbon interaction in Cu. Several steps involved in the graphene growth mechanism in Ni are described below.

1st step: Chemisorption of hydrocarbon occurs on the metal surface.
2nd step: Dissociation of hydrocarbon (dehydrogenation) on metal surface.
3rd step: Dissociated carbon atoms diffuse in to the bulk of the metal.
4th step: Diffusion of carbon atom from the bulk to the surface.
5th step: Precipitation/segregation process for graphene formation during cooling.

The final step happens only when the dissolution of carbon atoms reach a saturation level for the nucleation to begin. The final step doesn't stop until the carbon concentration in bulk comes to an equilibrium state even if the carbon supply stops.

Blakely's group has reported that in Ni, monolayer formation occurs first, followed by segregation and forming graphite.[16]

In Cu, due to low carbon solubility, the growth mechanism is surface mediated-adsorption process. The growth starts immediately after the dissociation of hydrocarbon and ends once the supply of hydrocarbon stops or the catalyst surface is completely occupied by graphene. Hence the growth mechanism is self-limiting. Figure 1.4 shows the graphene growth mechanism on Cu and Ni.

Metal	Carbon solubility (atom%) at 1000 °C
Co	3.41
Ni	2.03
Cu	0.04
Ru	1.56
Rh	0.89
Pd	5.98
Ag	0.01
Re	4.39
Ir	1.35
Pt	1.76
Au	0.01

Table1.1: Carbon solubility of transition metals at 1000°C.[17]

CVD growth of graphene or graphite on the surface of transition metal substrates such as Ni, Cu, Ru, Ir, Cu, and others, is studied.[18,19] Among several such metal catalysts, CVD growth on Cu and Ni is promising in terms of higher efficiency and scalability.[19-20] In case of Cu, it favours monolayer growth but Ni favours multi-layer graphene formation. Graphene grown on Ni surface generally results in non-uniform layer numbers. Therefore, one possibility in controlling the layer number would be to choose Cu-Ni alloy substrate. The addition of controlled amount of Ni to Cu can enhance the carbon solubility and additional layers can be achieved.[21]

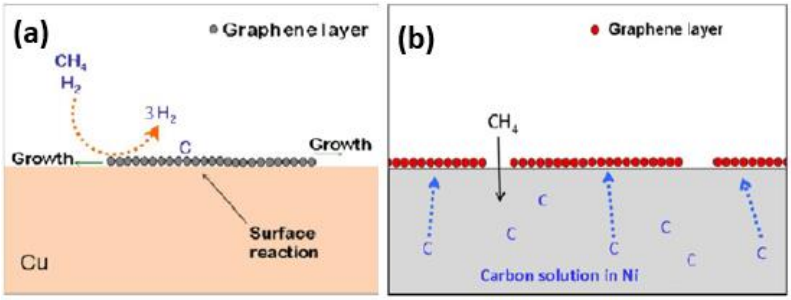

*Figure 1.4: Pictorial depiction of graphene growth mechanism on Cu **(a)** & Ni **(b)**.*[22]

1.3 Phase diagram of Cu and Ni

A Phase diagram is the representation of thermodynamic data in a graphical form. Phase diagrams are always used when designing an alloy or other metal substrates. Figures 1.5 & 1.6 show the binary Cu-C and Ni-C phase diagrams and their reported carbon solubility. It also depicts the interaction of carbon in these metals at elevated temperatures.

There are several reports on understanding the solubility of C in Cu.[23,24] None of such reports showed any carbide phase in the Cu-C equilibrium phase diagram. The phase diagram clearly shows the low carbon solubility of Cu. However, the accurate carbon solubility in Cu is still unknown. Figure 1.5 shows three different diagrams illustrating distinct carbon solubilities, however the methods used was not so accurate for determining the solubility of carbon in metals. López et al reported that the carbon solubility in Cu is within 0.04%, which was measured using combustion analysis.[24] By measuring the combustion of metals in air, McLellan et al reported that the C solubility in silver, gold and copper is about 10 ~ 70 ppm.[23] Mathieu *et al* reported that the carbon solubility of silver, copper and gold is within the order of 10^{-1} ppm, which was measured using Radiochemical methods.[25] All these reports suggest different observations in their solubility values and are not accurate. All these measurement methods are sensitive to factors such as surface carbon contamination on metals and purity of metals make these estimation tough. Hence it's difficult to quantify, rationalize and give the exact carbon solubility in Cu.

Figure 1.6 (a) and (b) show the binary phase diagram of Ni-C system. Ni forms metastable carbide phase at higher temperature.[26] Most of the growth conditions in CVD is operated at 1000^{o}C. The phase diagram indicates that the carbon solubility is ~2.7 at% at the eutectic point (1600 K) and 0.9 at% at about 900 K. which is greater than Cu.[26] During the cooling process, the carbon solubility is reduced and graphene layer gets precipitated.

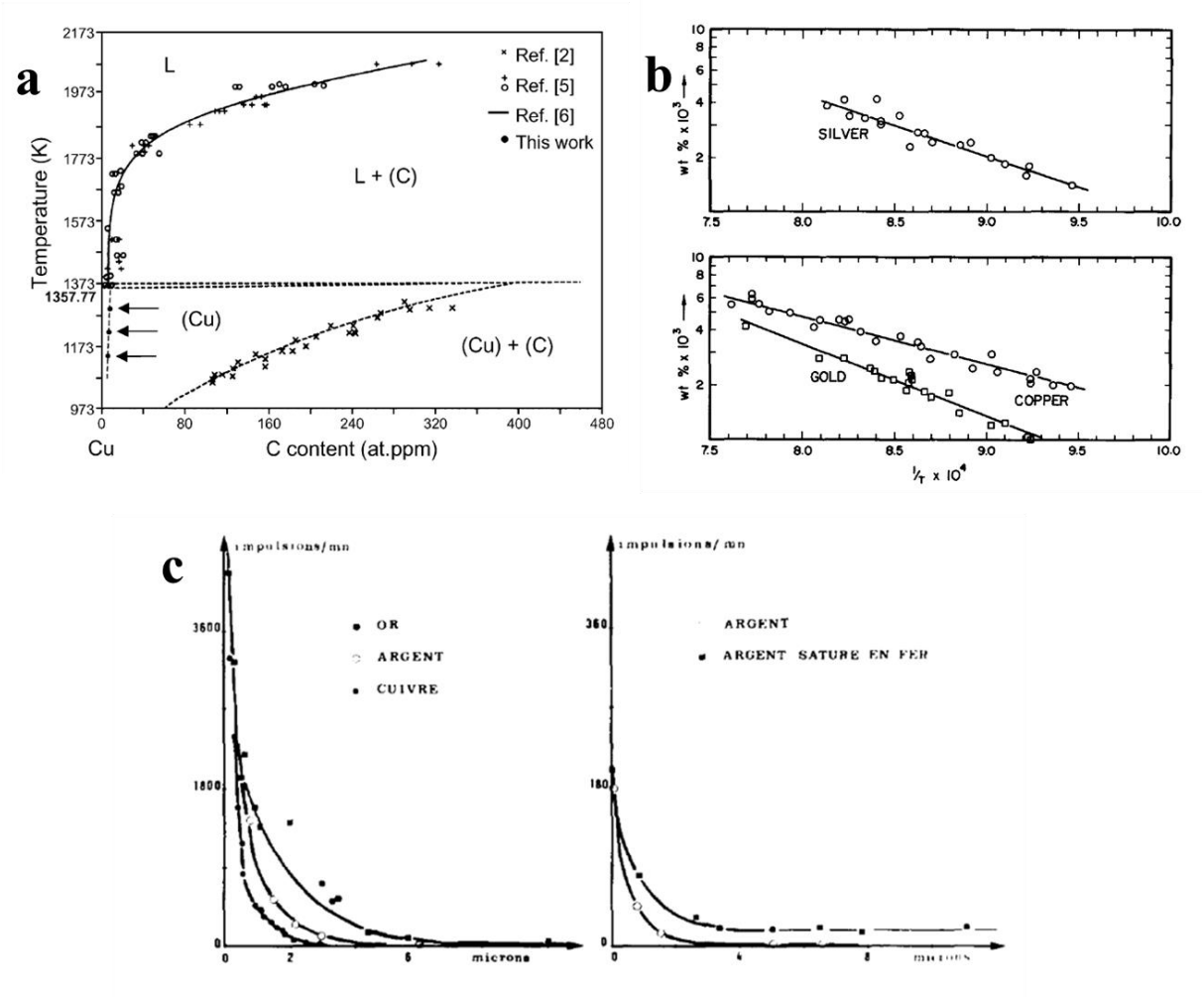

Figure 1.5: Binary phase diagram of Cu-C system from different reports: (a) G.A. Ropez et al[27]; b) R. B. McLellan et al [23]; c) G.Mathieu et al.[25]

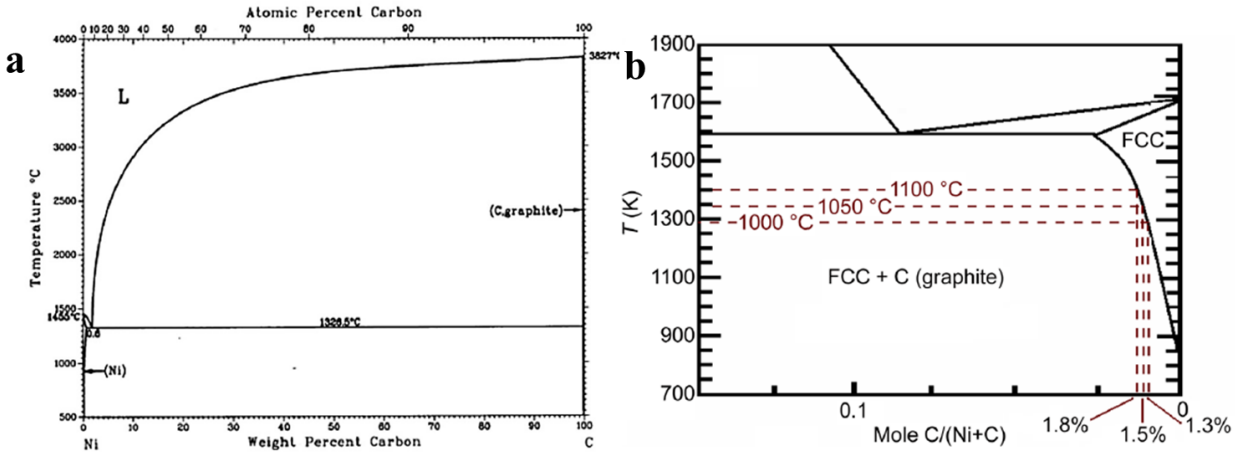

Figure 1.6: Binaryphase diagram of Ni-C system, from different reports.[26]

1.4 Cu-Ni alloy substrate for bilayer graphene growth

The low carbon solubility of Cu limits its use for the growth of large area multi-layer graphene and very high carbon solubility of Ni results in non-uniformity in the graphene layer numbers. Hence Cu-Ni alloy can be an alternative substrate to deal with this problem. The addition of Ni to Cu can enhance the carbon solubility. At elevated temperatures, Cu and Ni can be mixed to yield a homogeneous alloy, which was an idea of Prof.Ruoff.[28] A variety of compositions of Cu and Ni can be used for making alloy foils and they have been tested in Prof. Ruoff's group for growing bilayer and multi-layer graphene.[28-29] It is believed that the synergistic play between the distinct carbon solubilities of Cu and Ni and known segregation phenomenon play a major role in the formation of high-quality uniform few-layer graphene.

AB-stacked bilayer graphene has attracted particular interest due to its tunable electronic band structure, and is highly promising for electronic and photonic based device applications. Although some efforts have been made towards synthesising bilayer and multi-layer graphene on Cu, it still remain as a challenge to achieve large area bilayer and multi-layer graphene.[30,31] Cu-Ni alloy can be a suitable substrate for bilayer and multi-layer graphene growth owing to its moderate and tunable solubility.[21,32] They are prepared by the heat treatment of Ni-plated Cu foils, and the Ni content can be precisely controlled by adjusting the thickness of the plated Ni layer on each side of the Cu foil. Different compositions of Cu-Ni alloy are commercially available, but they contain elements other than Cu and Ni. Typical examples are '90-10', '80-20', and '70-30', which indicate the approximate atomic percentages of Cu and Ni, respectively.

1.5 Monocrystalline Ni (111) as catalytic substrate for graphite growth

Polycrystalline Ni substrate has been widely used for graphene growth.[15] However with polycrystalline Ni, the growth of single-layer and bilayer graphene is difficult to achieve. The challenges faced while growing multi-layer graphene on polycrystalline

Ni foil are, controlling the number of layers and uniformity. The grain boundaries in a polycrystalline Ni foil act as graphene nucleation sites, hence the graphene layers formed after carbon precipitation is non-uniform or inhomogeneous. Therefore, high quality graphene growth on polycrystalline Ni has been not realised yet. The exploration of graphene growth on monocrystalline Ni is very interesting. Ni (111) surface is a lattice matched surface close to graphite (the hexagonal lattice constant is 2.497 Å for Ni (111) and 2.46 Å for graphite).[33] From previous investigations of graphene growth on Ni (111) surface,[34] Blakely's group has investigated the mechanism of carbon precipitation on single-crystalline Ni surfaces with the help of low energy electron diffraction (LEED) and Auger electron spectroscopy (AES) [14,16, 35,36]. Figure 1.7 depicts the mechanism of graphene growth on monocrystalline Ni (111) and polycrystalline Ni substrates.[37] Ni (111) has advantages over polycrystalline Ni, because it is free from grain boundaries and perhaps has a lower density of other types of defects like step edges.[14] Ni (111) might be a better substrate for obtaining single crystal multi-layer graphene. But, this is unproven and needs further investigations.The LEED study has shown that the precipitated carbon atoms in Ni (111) preferentially follow graphite's lattice structure with proper epitaxy.[38] This is possible because of the close lattice match between Ni (111) surface and graphite. In addition, the scanning tunnelling microscopy (STM) image obtained for precipitated carbon layers on Ni (111) showed a three-fold symmetric pattern and is similar to that of highly oriented pyrolytic graphite (HOPG). It follows an ABAB-type stacking order.[39] Hence, from all these discussions it's clear that Ni (111) can act as a suitable substrate for the growth of multilayer graphene/graphite.

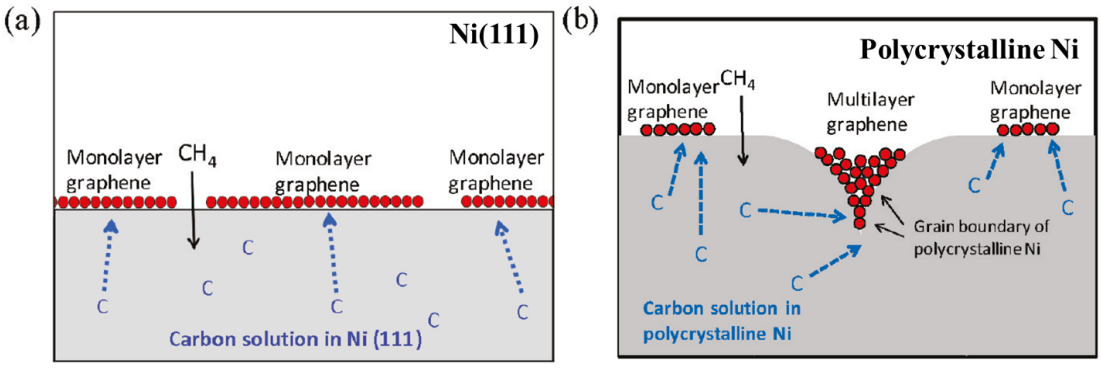

Figure 1.7: Schematic of graphene growth mechanism on (a) Ni (111) and (b) polycrystalline Ni surface.[37]

1.6 Phenolic resin as graphitizable carbon precursor

In most of the graphene growth processes, the carbon precursor has to be adequately volatile. Hence, gaseous precursors such as methane, ethylene, acetylene, and others have been widely used as precursors in CVD.[10,40] For liquid and solid precursors, volatility can be increased by reducing their intermolecular forces, which may result in dimer, oligomer or polymer formation. However, reports suggests that carbon precursors in their solid form such as polymers could be potentially used.[41] In our project, we have used methane as the carbon source for single-layer and bilayer graphene growth on Cu and Cu-Ni alloy foil. But for growing multi-layer graphene/graphite, phenolic resin polymer has been used as the carbon precursor.

Figure 1.8 shows the structure of phenol formaldehyde resin polymer and its formation from monomers. Phenol formaldehyde resin is a synthetic polymer obtained by the condensation reaction between phenol or substituted phenol with formaldehyde. They are widely being employed for the production of circuit boards, moulded products including billiard balls, laboratory countertops, among others. Phenolic resin has also been used widely as a binder material during the graphitization process of petroleum coke.[42]

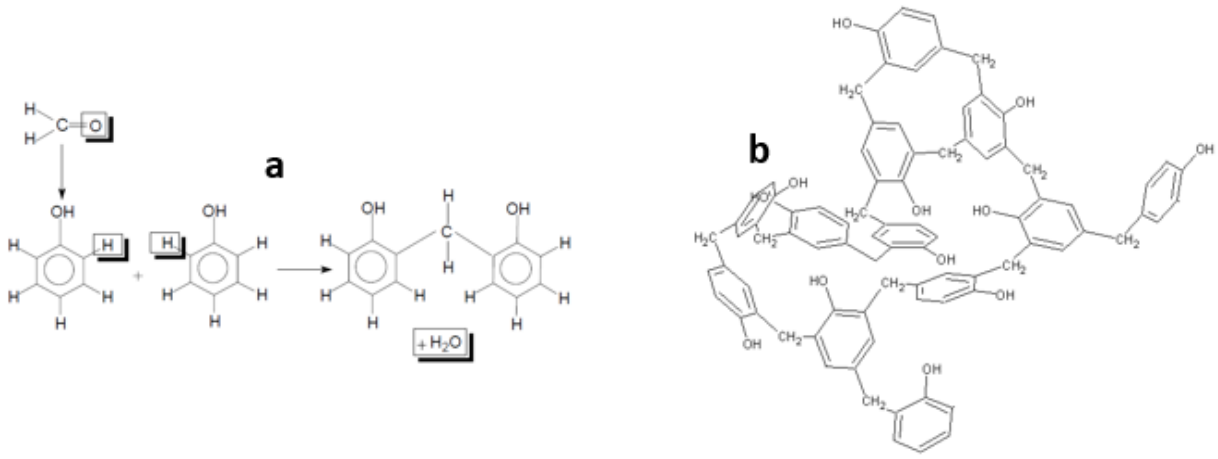

Figure 1.8: Formation of phenolic resin (PR) from monomers (a); and its structure (b) (Wikipedia accessed on 2nd March, 2016).

The mechanism of carbonization of phenol formaldehyde resin was reported by Yamashita et al. in early 1980's.[43] Figure 1.9 shows the schematic of the carbonization of phenol formaldehyde resin as understood through the use of isotope studies with deuterium and ^{13}C. A temperature below 340°C leads to water elimination and at a temperature above 400°C, moities are generated that are crucial for graphite formation (methane, hydrogen, carbon monoxide and carbon dioxide). Among them, methane is an important precursor molecule for graphene/graphite formation and is derived from methylene groups that doesn't participate in dehydration reactions.

There are reports showing the catalytic graphitization of phenolic resin with the aid of ferric nitrate catalyst.[44] They further show that the catalytic graphitization transforms phenolic resin to a highly ordered 'graphitic' carbon (onion-like carbon particle and bamboo-shaped carbon nanotube).

Following the above study, we considered phenolic resin as our carbon precursor and Ni (111) as the potential catalyst for thin-layer graphite growth.

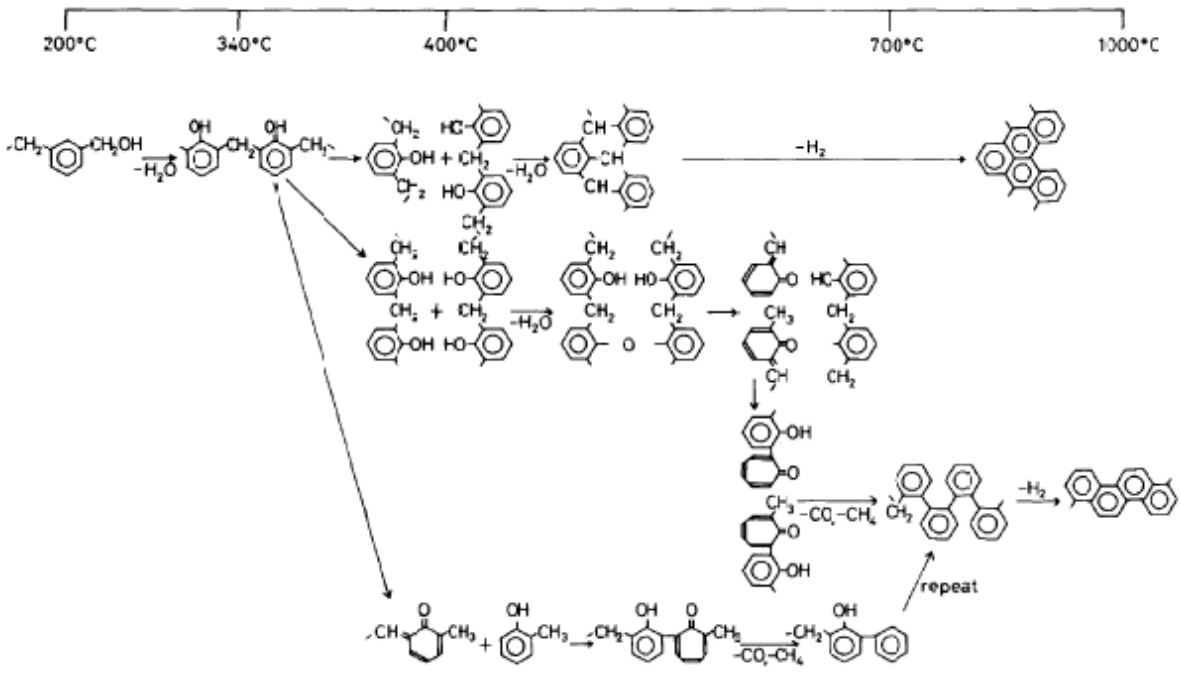

Figure 1.9: A schematic illustration of the carbonization mechanism of phenol formaldehyde resin.[43]

Chapter 2

Experimental and Characterization Techniques

2.1 Experimental Methods and Techniques

2.1.1 Chemical Vapour Deposition (CVD)

Chemical Vapour Deposition (CVD) involves the reaction of precursor molecules in the vapour phase on a heated substrate under low pressure or atmospheric pressure conditions. This technique helps depositing thin films (such as graphene or graphite) in assistance with transition metal catalysts.[10] The growth of graphene films on copper foils by CVD is widely used for the production of large-area graphene due to the advantages of low cost, ease of graphene transfer, and high quality.[10]

Hydrocarbons have been used for the synthesis of graphene and graphite. The solubility of carbon in metal catalysts along with CVD conditions determine a role in the growth mechanism and perhaps, in ultimately controlling the graphene layer number.[15]

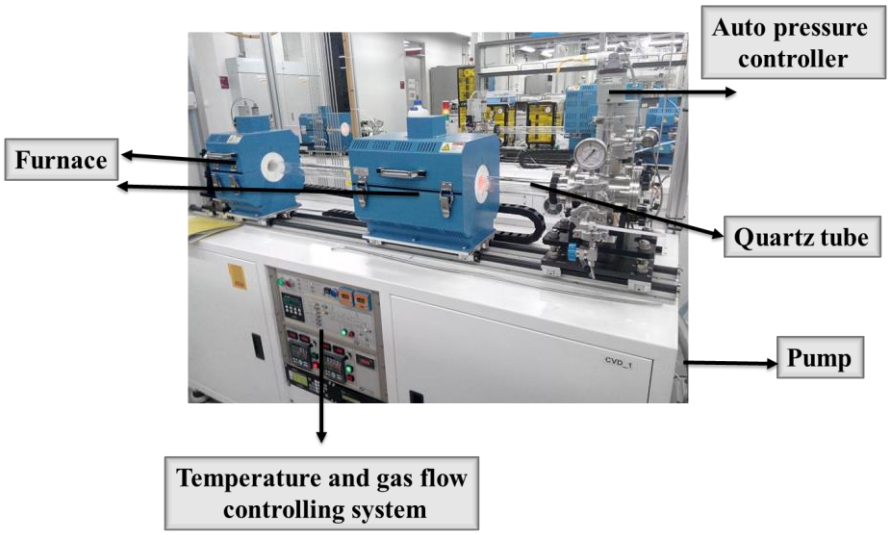

Figure 2.1.1: Chemical Vapour Deposition (CVD) setup used for this project.

2.1.2 Spin Coating

Spin coating technique is used for the deposition of thin films. A small amount of polymeric solution is dripped onto the centre of a substrate that is spun at high speed (usually 1000-8000 rpm). Factors contributing to the film properties are rotational speed (rotations per minute), acceleration, deceleration and fume exhaust.

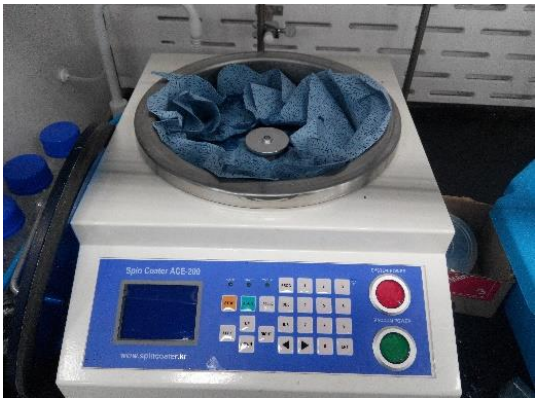

Figure 2.1.2: Spin Coater ACE-200 used in this project for depositing thin polymer films.

2.1.3 Oxygen Plasma Treatment

Oxygen Plasma treatment is an effective method for removing the surface impurities and contaminants. Organic contaminants can be converted to products such as H_2O, CO_2, and lower molecular weight hydrocarbons. As these compounds possess relatively high vapour pressures, they are evacuated from the chamber during the plasma etching process and this can substantially clean some surfaces.[45]

Figure 2.1.3: Typical oxygen plasma etching system.

2.1.4 Transfer Process

2.1.4.1 Polymer-assisted transfer of films

Graphene formed on the metal substrate needs to be transferred onto silicone (Si/SiO_2) for detailed analysis. One of the reported transfer method involve the use of PMMA [Poly (methyl methacrylate)]-assisted wet transfer route.[46] Figure 2.1.4 shows the schematic representation of polymer-assisted (PMMA), wet transfer method of transferring graphene. On one side of the substrate (graphene on metal), usually PMMA solution is spin coated, followed by an oxygen plasma treatment that removes graphene present on the other side. Then, the PMMA/graphene/copper stack is allowed to float on the surface of the etching solution, ammonium persulfate [$(NH_4)_2S_2O_8$] in water. Once the etching is completed, the graphene/PMMA film is washed using D.I. water 2-3 times. The floating graphene film is then transferred to a desired substrate (Si/SiO_2) by taking out the film carefully from the water surface. The graphene film on Si/SiO_2 is then allowed to dry naturally for several hours. Once the film is dried, it is again coated with PMMA solution to make the graphene surface relax and flat on the Si/SiO_2 substrate. Finally the PMMA/graphene/Si/SiO_2 is dipped in acetone bath for removing PMMA. After several cycles of washing with PMMA, the graphene film on substrate is available for characterizations.

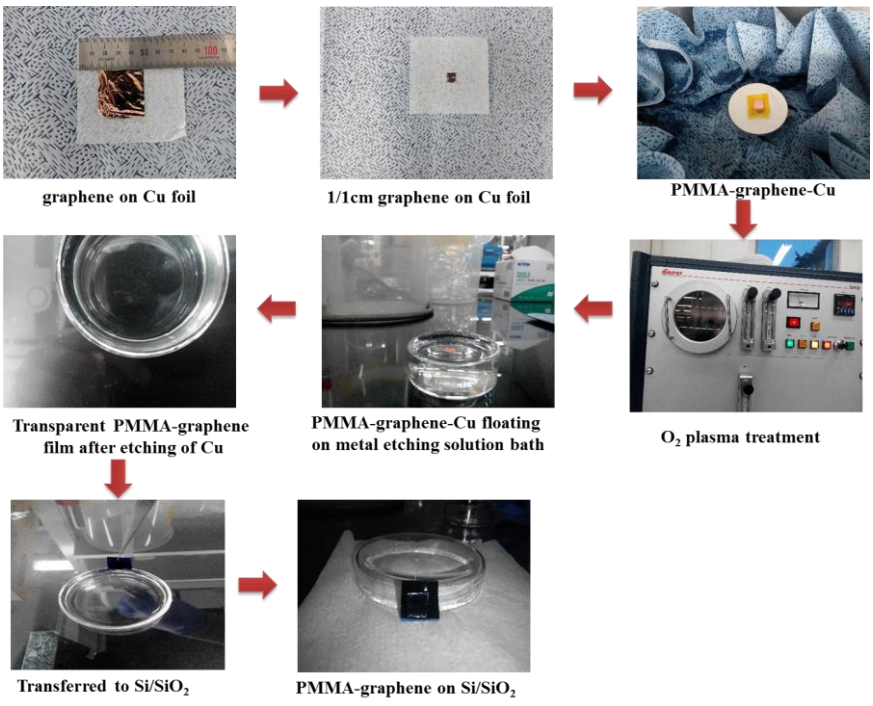

Figure 2.1.4: Schematic representation of polymer (PMMA) assisted wet transfer method of graphene.

2.1.4.2 Bubbling transfer of films

Bubbling transfer of films of monolayer and few-layer graphene to arbitrary substrates is a non-destructive technique available.[47] Figure 2.1.5 shows the schematics of the bubbling transfer (an electrochemical method) of graphene**.** The CVD-grown graphene on Cu is first spin-coated with polymethyl methacrylate (PMMA). The PMMA/graphene/Cu is then dipped into an electrolyte (NaOH aqueous solution) and used as the cathode of an electrolytic cell with a constant current supply. Pt electrode serves as the anode. A reduction of H_2O takes place at the cathode, generating H_2 bubbles. The reactions can be represented as follows:

Cathode:

$$2\,H_2O + 2\,e^- \rightarrow 2\,OH^- + H_2\uparrow$$

Anode:

$$2\,OH^- \rightarrow H_2O + 2\,e^- + 1/2O_2\uparrow$$

Net Reaction:

$$2\,H_2O \rightarrow H_2 + 1/2\,O_2 + H_2O$$

As a result of formation of a large number of H_2 bubbles at the interface between the graphene and Cu substrate, the PMMA/graphene layer slowly detaches from the metal substrate in a short time. PMMA is then removed using acetone, and the films can be transferred to the desired substrate.

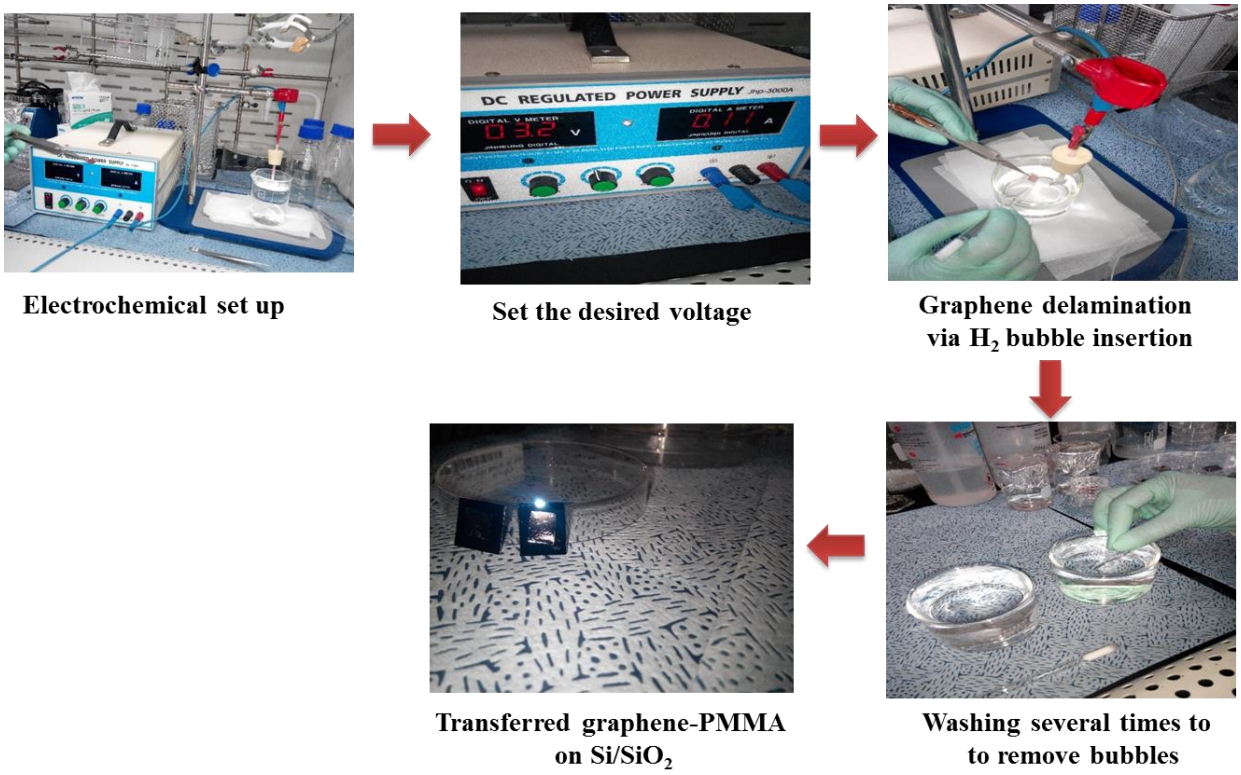

Figure 2.1.5: Schematic representation of bubbling transfer (an electrochemical method) of graphene.

2.2 Characterization Techniques

Various characterisation techniques commonly used for the detailed study of carbon materials are Raman spectroscopy , Optical microscopy , scanning electron microscopy (SEM), X-ray photoelectron spectroscopy (XPS) and atomic force microscopy (AFM). Among all these techniques, Raman is considered as the most versatile and is predominantly used tecnique for studying carbon materials. Being a non-destructive technique it offers other advantages such as sample integrity. Here, the materials subjected to the characterisation study are films of graphene and thin layer graphite grown on various substrates. Raman gives the information regarding the bond structure and estimation about graphene film thickness etc... Each method gives a different insight about the structure and performance of the material. Various techniques will be explained briefly in the next section.

2.2.1 Optical Microscopy

Surface morphology of the graphene and graphite films can be obtained from optical microscopy after transferred to a Si/SiO_2 substrate and images are directly recorded. Refractive lenses are used to focus the reflected light from the sample onto the detector. This technique can give idea about the film thickness and uniformity, based on the colour contrast with respect to Si/SiO_2 substrate. The underlying principal being thin film interference. Graphene monolayers generally are highly transparent and thin, but the thickness increases as the number of layers increases. On the optic micrograph the graphene and few-layer graphite can be distinguished clearly on the basis of colour as seen from Figure 2.2.1: ***(a)***. But the actual number of graphene layers in graphite is difficult to determine by this method.

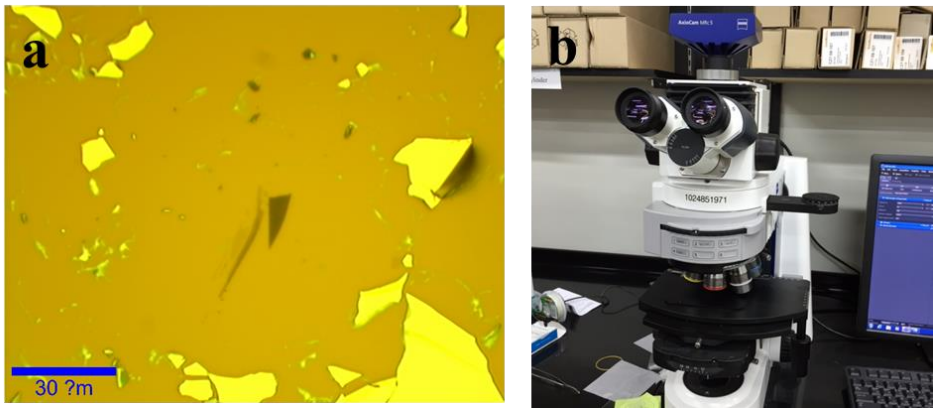

Figure 2.2.1: a) Optical microscopy images of micromechanically exfoliated samples of graphene and thin layer graphite films on Si/SiO_2; b) Zeiss Optical microscope used for generating optical images in the lab.

2.2.2 Scanning Electron Microscope (SEM)

Scanning electron microscope (SEM) is a useful technique to see the surface morphology of the specimen in a much higher resolution (typically in micron scale), and it clearly shows characteristic film defects in a material. Focused high-energy electrons are used for creating an image by detecting the backscattered or secondary electrons from the surface of the sample. Main components of a typical SEM include electron lenses, sample stage, electron gun, detectors and a display. -

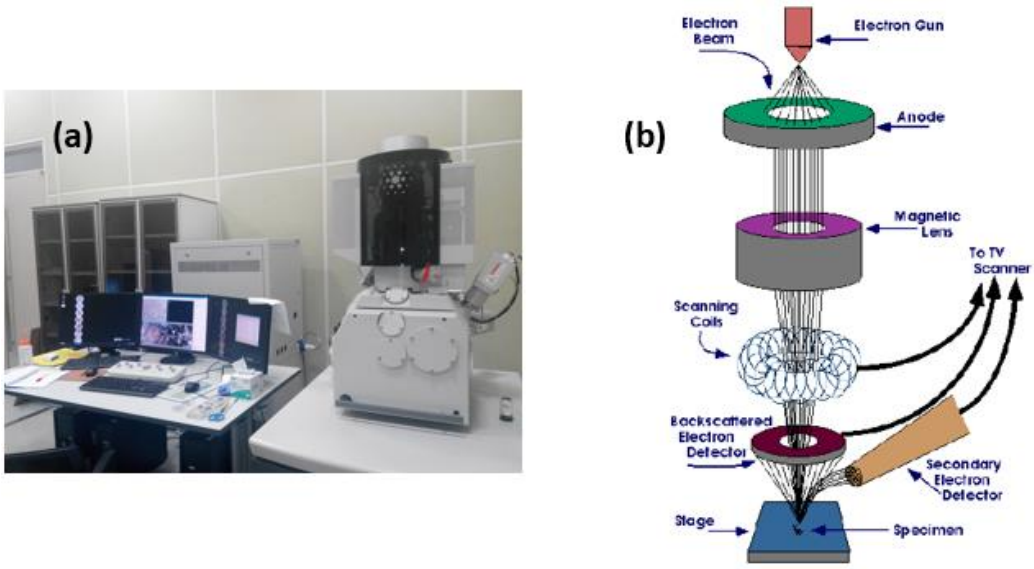

Figure 2.2.2: a)Picture of SEM set up used for this project; b)SEM Working principle (ref: https://www.purdue.edu/ehps/rem/rs/sem.htm)

2.2.3 Raman Spectroscopy

Raman spectroscopy plays a significant role in the structural characterization of graphitic materials and is an important tool for understanding the behaviour of electrons and phonons in these materials.

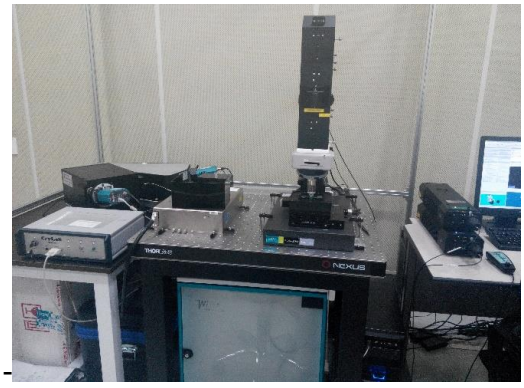

Figure 2.2.3: Raman spectroscopy set up used for this project.

This method uses a monochromatic laser excitation for probing the sample. The incoming laser light loses some energy which is used for exciting vibrational modes (or phonons) present in the material. Raman scattered photons possess lower energy than the initial photons and the difference in energy after scattering is observed as a

Raman shift. Raman shift corresponds to the energies of vibrational modes that in turn are indicative of the structure of a material. Raman shift is reported as wave number in units of cm^{-1}.

Raman spectrum captures the electronic structure of graphene and it clearly evolves with the number of layers. There are three distinct peaks correlated with various vibrational or phonon modes in graphene, referred as D, G and 2D (G'). Both the G (~1587 cm^{-1}) and D (~1350 cm^{-1}) modes correspond to bond stretching modes. The G mode appears due to the in-plane vibrational mode (between any pair of sp^2 hybridized carbon atoms), whereas D mode originates from a vibrational mode in the sp^3 bonded carbon. Often broadening of the bands can be attributed to their amorphous nature (short range ordering of the layers). The D peak is generally forbidden in pristine graphene, but becomes an allowed one when defects are present. Therefore, the intensity of D peak is directly connected with the amount of defect in a material. The 2D peak (~2700 cm^{-1}) is an overtone of the D peak, which is believed to be originated from zone-boundary vibrational mode, consists of four different peaks. It shows up even if there's no D peak in the spectrum. In graphene monolayer, only one of those peaks is predominant and is sharp. Depending upon number of graphene layers, G and 2D peaks changes its shape, position and intensity.[48]

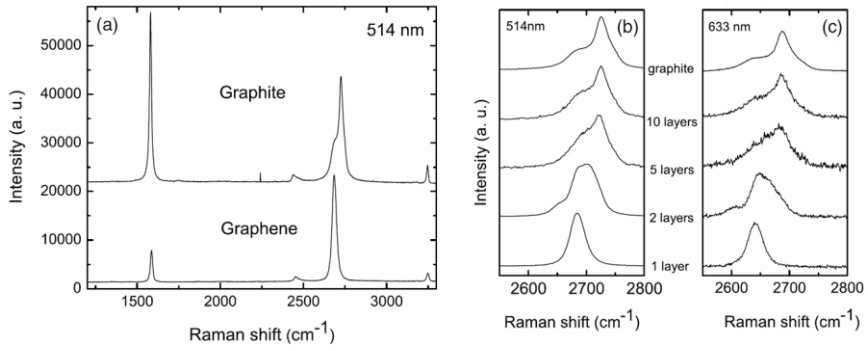

Figure 2.2.4: (a) Raman spectra of bulk graphite & graphene at 514 nm; (b) Evolution of the spectra at 514 nm & (c) at 633 nm with the number of layers.[48]

2.2.4 X-ray photoelectron spectroscopy (XPS) Depth Profiling

XPS depth profiling technique gives subsurface information of a material. The spectra are acquired using an ion beam by etching the surface layers for a short period of

time. Each etching cycle leads to the exposure of a new surface and the collected spectra gives information about the compositions that it contain. A quantified information along with layer thicknesses can be obtained from this technique.

2.2.5 Atomic Force Microscopy (AFM)

AFM is used to characterise the surface morphology of a film and also helpful in high resolution topographical imaging of nanomaterials. The images are generated based on the forces between the AFM tip and the sample. The image resolution is affected by the sharpness of the AFM tip, i.e., when the tip comes in the vicinity of sample surface, a deflection is generated in the cantilever due to the force generated between the sample and the tip. It is measured by reflecting a laser beam onto a photodetector. The surface topography of a material essentially determines the cantilever deflection. AFM relies on a feedback loop, a piezoelectric scanner underneath the sample maintains a constant force on the cantilever and helps acquiring the surface topography in all directions.

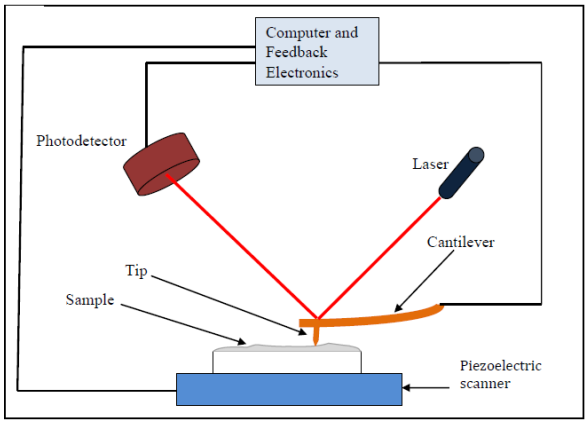

Figure 2.2.5: A Schematic of Components of the AFM system.

2.2.6 X-ray diffraction (XRD)

XRD is a non-destructive characterisation technique primarily used for identifying the phase in a crystalline material. It can give information about the unit cell dimensions. The sample is hit by X-ray beam and the emerging diffracted beams are detected. The diffraction intensity is dependent up on the interaction of the beam with the sample. The diffraction pattern is a plot of intensity vs. the scattering angle, 2θ.

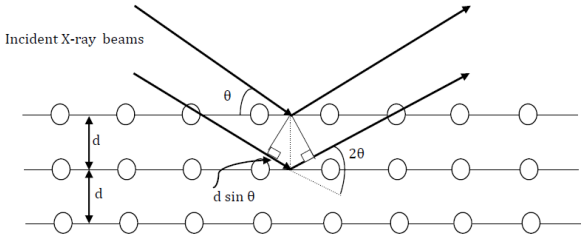

Figure 2.2.6: Schematic representation of the diffracted beams.

XRD patterns are generated from constructive interference, and it occurs only for certain θ's related to planes (hkl), where path difference is an integral multiple (n) of wavelength as determined by the Bragg's equation:

$$n\lambda = 2d\sin\theta$$

Where n is the order of the diffracted beam, λ is the wavelength of the incident wave, d is the interplanar distance and θ represents the scattering angle.

2.2.7 Thermogravimetric Analysis (TGA)

TGA is used for understanding the thermal stability and composition of a material. TGA measures the weight change in a material as a function of temperature or time in a controlled environment. This technique is widely implemented for the characterization of materials used in environmental, petrochemical and pharmaceutical applications. A TGA set up consists of a sample pan placed in a furnace with a supporting precision balance. The sample environment is controlled by gaseous atmosphere (inert or reactive). The heating rate is programmable and can operate with various gases.

Figure 2.2.7: TGA set up used for characterising the thermal degradation of Phenolic resin.

Chapter 3

Experimental Details, Results and Discussions

3.1 Experimental Details

3.1.1 Thin-layer graphite formation by high temperature annealing

All the reactions were performed inside a chemical vapour deposition (CVD) chamber. Various concentrations of polymers such as polyvinyl alcohol, polystyrene were prepared with ethanol (solvent) and spin-coated over metal substrates (Cu and Ni). But various concentrations of phenolic resin (50 mg/ml to 500 mg/ml) were made using tetrahydrofuran (THF) solvent. These solutions were spin coated several times on to metal substrates like mono crystalline Ni (111), polycrystalline Ni foils and also on Si/SiO_2 containing graphite seed layer with a rotational speed of 3000 rpm for few seconds. This process was repeated several times followed by annealing at ~100^oC for 20 minutes to ensure complete removal of the solvent. The Ni (111) foil with phenolic resin spun coat was then kept inside a CVD chamber for high temperature annealing. The annealing was performed at 1000°C with 100 sccm Ar and 20 sccm H_2 for 6 hrs, followed by slow cooling up to room temperature. A pressure of 10 torr was maintained throughout. The sample was analysed using all the available characterization techniques (Optical microscopy, Raman spectroscopy, XRD, SEM, AFM and XPS).

3.1.2 Chemical Vapour Deposition (CVD) of graphene

Graphene growth was carried out with the help of a low pressure CVD system. A 20 μm thick polycrystalline Cu foil was used for single-layer graphene growth. Prior to conducting growth, the metal foil was dipped in acetic acid for some time to remove the surface oxide layer and other contamination. The foil was then dried with blowing N_2 gas and was kept inside a CVD chamber. The Cu foil was annealed at 1050^oC for

2 hrs in 30 sccm of H_2 to remove the surface oxide and to make the metal surface flat to promote graphene growth. Then, a 10 sccm flow of CH_4 was introduced into the chamber for 30 minutes, and the sample was fast-cooled by sliding the furnace from the heating zone. Following which, the graphene on Cu was transferred to a silicone (Si/SiO_2) substrate by PMMA or electrochemical transfer method for detailed analysis. A 120 µm thick Cu-Ni (90/10) alloy was used to grow bilayer graphene. The growth conditions were similar to that of monolayer graphene growth except that a pressure of 10 torr was maintained throughout.

3.2 Results and Discussions

3.2.1 Thin-layer graphite synthesis from polymer carbon precursors

Figure 3.1 (a) shows the SEM image of annealed sample of copper foil with PVA drop casted on it. No continuous film was seen on the foil, nonetheless some carbon patches were observed. The carbon sample was transferred to Si/SiO_2 to perform the Raman measurement and the results are shown in Figure 3.1 (b). Raman spectra consist of D and G band and a very small 2D band. To achieve continuous film growth, we increased the annealing time and PVA concentration. But we observed only large-sized carbon patches even after multiple trials. Similar results were followed with polystyrene polymer, too.

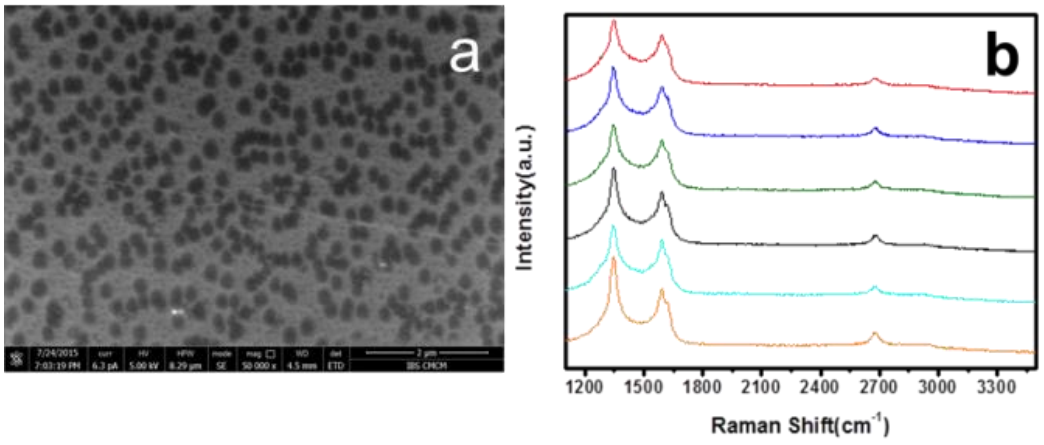

Figure 3.1: (a) SEM image of annealed sample (copper foil with PVA), (b) Raman spectra of the same sample after transfer, at different positions.

Following which, we tried to use the cross linked organic polymer molecule, phenolic resin (phenol-formaldehyde resin) as our carbon precursor. The details about this polymer are described in the introduction section. Prior to working with phenolic resin, we performed thermo gravimetric analysis (TGA) to check the decomposition temperature of the polymer. The TGA analysis of phenolic resin is shown in Figure *3.*2. The polymer was heated up to 1000°C with a heating rate of 10°C/min under nitrogen atmosphere. It seems that the maximum weight loss was observed between a temperature range of ~100-500^{o}C. After which, the weight remained almost stable and 10-20% weight was retained.

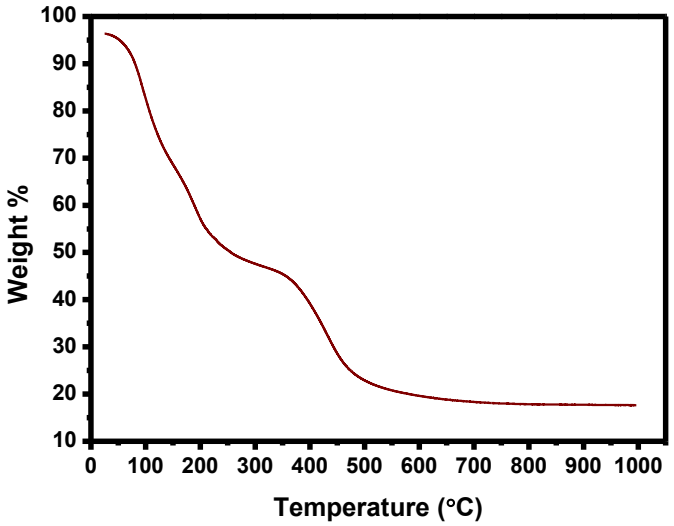

Figure *3.*2: *Thermo gravimetric analysis of phenolic resin in N_2 atmosphere.*

Phenolic resin was then used as carbon precursor, aimed at growing graphene/graphite. High temperature annealing was performed in a mixed environment of Ar and H_2. Figure 3.3(a) shows the SEM image of phenolic resin derived carbon on copper foil, SEM micrograph can be seen as a non-continuous carbon film on copper foil. The film was then transferred onto Si/SiO_2. Raman spectra of the transferred film showed broad and merged peaks of D and G band and no 2D band, suggesting that the film obtained was neither graphene nor graphite. Different growth conditions were tried with increasing the concentration, annealing time and pressure, but similar results were obtained.

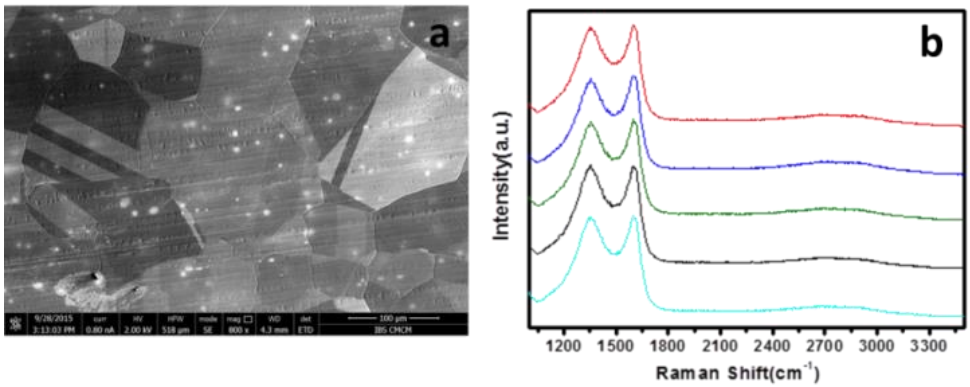

Figure 3.3: (a) SEM image of the annealed sample (copper foil with phenolic resin), (b) Raman spectra of the same sample after transfer, at different positions.

Similar experiments were done using polycrystalline Ni substrate. Phenolic resin was spin coated directly on the Ni foil and was annealed for 1 hr in Ar and H_2. Figure 3.4(a) represents SEM images of the annealed Ni foil having phenolic resin, which showed a clear contrast difference. After Raman measurements, it was found that the dark region formed on the Ni foil is graphite and the bright region is Ni foil. The Raman spectra are shown in Figure 3.4(b). The Raman spectra showed sharp G peak and broad 2D peak and no D peak. This is a typical character for the Raman spectra of few layer graphene or graphite (a typical Raman spectra of graphite, with 532 nm laser, shows three distinct peaks, a D band (~1350 cm^{-1}), a G band (1580 cm^{-1}) and a 2D band (2700 cm^{-1})). The absence of D peak indicated that the formed graphite has minimum defects. The graphite formation on Ni foil can be explained using precipitation mechanism. That is, during the carbonization process there might be some carbon which was dissolved in Ni due to the high solubility of carbon in Ni. During the cooling process, the carbon layers separated out to the Ni surface and formed graphite. Nonetheless, the graphite layers formed on the poly crystalline Ni surface is not uniform and the layer numbers are different at different positions.

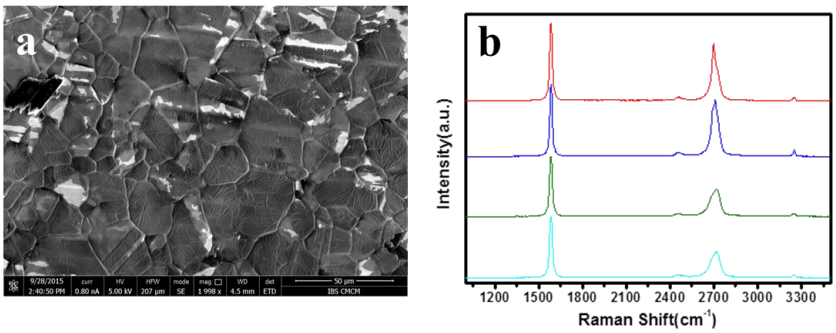

Figure 3.4: *(a) SEM image of Ni foil with phenolic resin, after annealing, (b) Raman spectra of the same sample at different positions.*

After optimizing of the growth conditions on different metal substrates such as Cu and Ni, it turned out that we were only able to grow graphite on polycrystalline Ni foil. However, there are several literatures regarding the growth of multi-layer graphene/graphite on Ni surface being non-uniform and with small grain sizes.[15] To achieve growth of very high quality few layer graphene or graphite, polycrystalline Ni substrate is not a good option. The grain boundaries in polycrystalline Ni foil act as graphene nucleation sites, thus precipitation of carbon atoms from the bulk to the surface is non-uniform. Hence, the layer numbers of the obtained film is also non-uniform over the whole area.[37]

Because of higher carbon solubility Ni is a better substrate than Cu for few layer graphene or graphite growth. However, the precipitation is thermodynamically driven and it can be controlled kinetically up to a certain extent. By employing the fast cooling rate, low temperature annealing and reducing the amount of carbon precursors, layer number control can be achieved.[15] It has been believed that the multi-layer domain formation can originate from several factors such as grain boundaries and defects in the polycrystalline Ni foil. Also, there's a very close match between the crystal lattices of graphene and Ni (111), the hexagonal lattice constant for Ni (111) is 2.497 A° and for graphene/graphite is 2.46 A°.[49] Therefore, growing graphene/graphite on single crystalline Ni surfaces can potentially yield high quality samples.

In this project, we were aimed at growing large-area graphite/graphene on the Ni (111) surface using phenolic resin. The Ni (111) surface is obtained from single crystalline Ni surface, which is quite expensive. However, the real motivation was to get the films with controlled layer number and large domain size.

The large-sized Ni (111) foil was prepared by the high temperature annealing of the polycrystalline Ni foil for a very long time. During annealing, Ni grain with the most stable orientation, (111), grows larger in size, thus we can achieve centimetre-sized grains having (111) orientation. It was investigated that using Ni (111) surface, highly oriented pyrolytic graphite (HOPG) can be synthesized.[39] We used this foil to grow high quality large area thin-layer graphite from phenolic resin. Figure 3.5 shows the XRD spectra of the lab made Ni (111) foil, it showed preferred (111) orientation at a 2θ value of ~44 degree, and the entire Ni foil consisted of centimetre scale grains having (111) orientation.

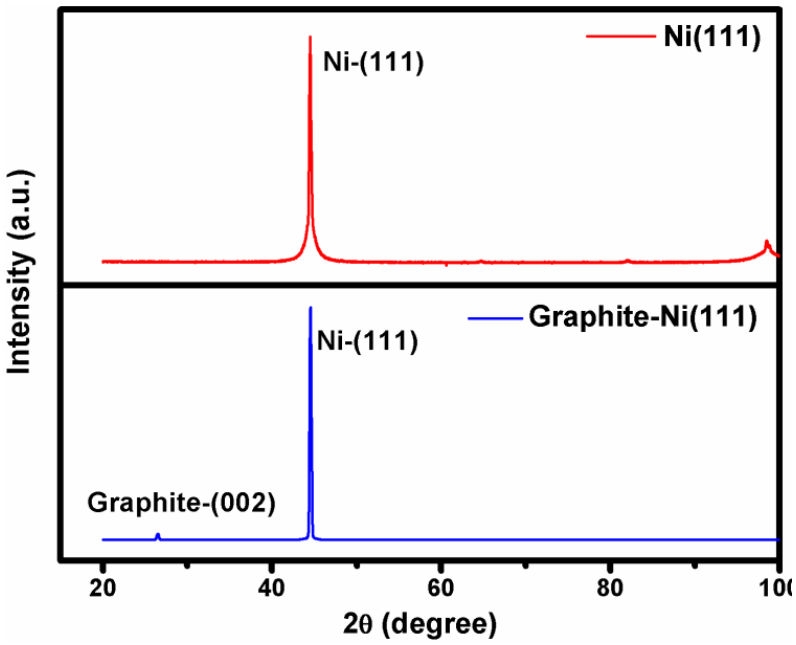

Figure 3.5: *(a) XRD spectra of bare Ni (111) and phenolic resin derived graphite on Ni (111).*

After characterizing the Ni (111) foil, a thin-layer of phenolic resin solution made in tetrahydrofuran (THF) was spin-coated several times at ~3000 rpm to deposit sufficient amount of carbon. Several concentrations like 50 mg/ml, 100 mg/ml and 500 mg/ml were made and used during the growth optimization. The spin coated samples were subjected to heating on a hot plate at 100^{o}C for 30 min. This was done for completely evaporating the solvent. The Ni foil was then inserted in to a CVD chamber for high temperature (1000^{o}C) annealing in a mixed atmosphere of Ar and H_2. We could not observe any carbon species during the initial stages of growth optimization using dilute concentration of resin. Whereas by slightly increasing the concentration (such as 50 mg/ml and 100 mg/ml), we started to observe few patches of thin graphitic layers. For 500 mg/ml concentration, uniform graphite film was formed on the metal surface. Further characterizations were done for the graphite formed from 500 mg/ml concentration of the resin. The XRD spectra of the graphite shows a clear peak of graphite, (002) plane at a 2θ value of ~26 degree along with Ni (111) peak at ~44 degree (Figure 3.5).

Figure 3.6 (a & b) show the SEM images of graphite formed on Ni (111) surface at different magnifications. The images clearly showed that the layer numbers are not uniform at some positions. This could be due to the non-uniform precipitation of carbon layers on the surface. Figure 3.6(c) shows optical image with positions from where the Raman spectra was taken, and the Raman spectra were represented in

Figure 3.6(d). From Raman spectra, it was apparent that the carbon material being formed is graphite and it manifested a typical spectra of graphite (a very high G band and a broad 2D band). There is no signature of a D band, indicating the minimal defect in the graphite structure. Nevertheless, from Raman measurements, it was seen that the layers were very thick. We did AFM measurement to figure out the exact thickness of graphite.

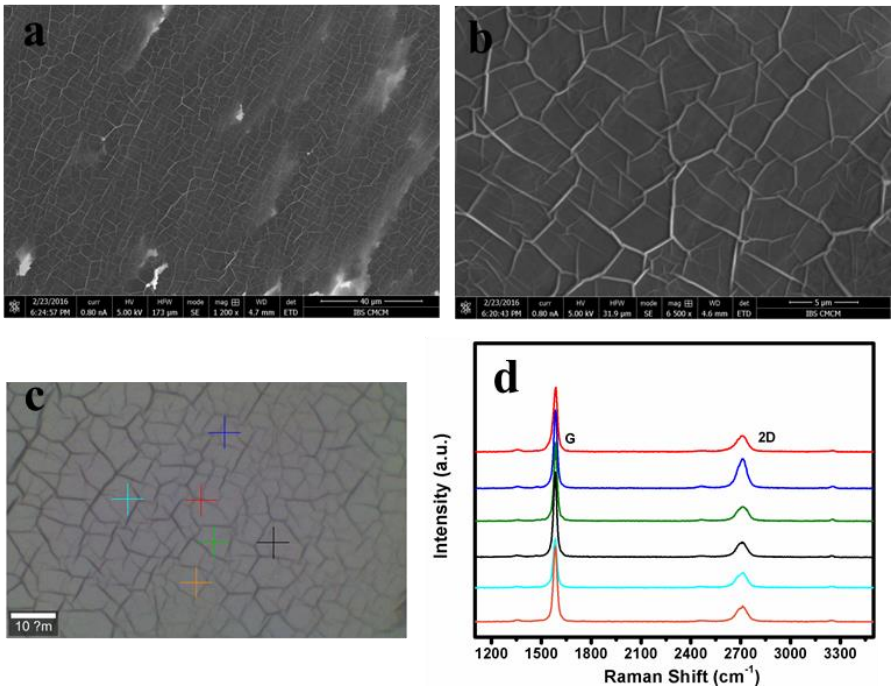

Figure 3.6: (a-b) SEM images of phenolic resin derived graphite on Ni (111) at different magnifications; (c-d) Raman spectra of graphite on Ni (111) at different positions.

AFM images of phenolic resin derived graphite and its height profile are shown in Figure 3.7 (a) and (b). AFM image was taken near the edges of the Ni (111) foil to get the height difference between Ni foil and graphite. From height profile, it was clear that the graphite is ~30-70 nm thick and the thickness is non-uniform. Therefore, further optimization is needed to control and reduce the layer numbers by having a control over the precursor amount, annealing time and cooling rate.

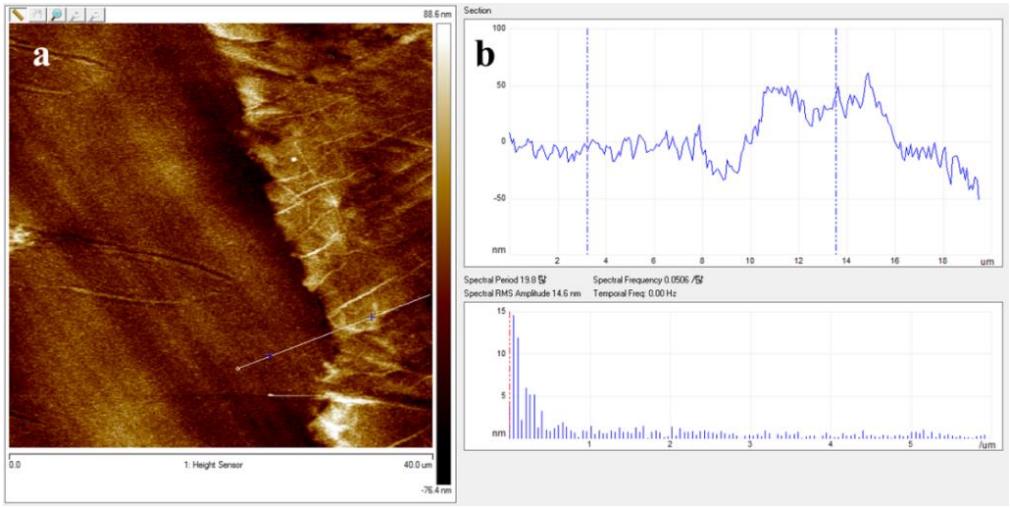

Figure 3.7: (a) -AFM data for phenolic resin graphite on Ni (111); (b) Height measured from AFM.

Raman mapping was also done over 20 µm/20 µm area of the sample and the obtained data is shown in Figure 3.8. The optical image shown in Figure 3.8(a) represents the Raman mapping region (indicated in a red square). Figure 3.8(b) shows map for 2D peak width, which is non-uniform over the whole surface, indicating the non-uniformity of graphite layers on the Ni (111) surface. The negligible I_D/I_G ratio in figure 3.8(c) indicates minimum defects in graphite. The I_{2D}/I_G ratio in 8(d) is <1, which indicates a higher intensity of G peak due to large number of layers in graphite.

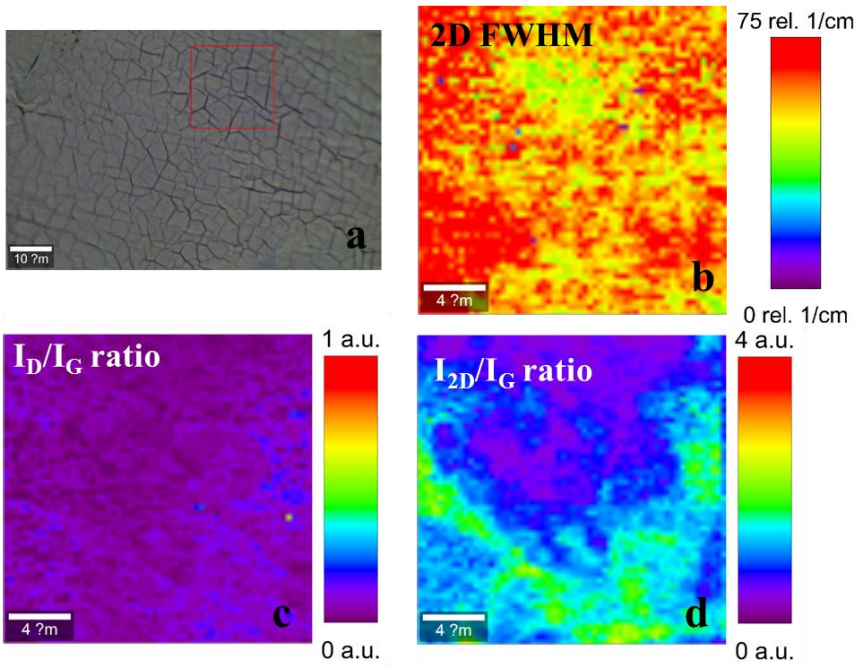

Figure 3.8: Raman mapping data for the phenolic resin derived graphite on Ni(111) foil; (a) Optical image of graphite showing the area chosen for mapping, in red square (20µm /20µm); (b) 2D FWHM map; (c) I_D/I_G ratio; (d) I_{2D}/I_G ratio of the specified region.

For lower concentrations of phenolic resin (50 mg/ml and 100 mg/ml), we were not able to observe any carbon species on the Ni (111) surface. However, for 100 mg/ml, after carefully weighing the Ni (111) substrate before and after the reaction, we frequently observed a weight difference of ~0.02-0.05 mg. No considerable weight difference was observed when the concentration was 50 mg/ml. The reason for such a weight difference of the foil is attributed to the dissolved carbon in the bulk of the Ni foil. For 500 mg/ml sample, there is sufficient amount of carbon species available that is dissolved in the Ni foil and precipitated out to yield graphite. Whereas for lower concentrations like 100 mg/ml, the carbon species might have dissolved into the foil, but the dissolution is not saturated enough to make it to the surface and form graphite. We thus observed tiny thin patches of carbon at some places. The number of graphene layers formed rely on the cooling rate and the carbon concentration being used. For studying the mechanism in more detail, we further analysed these samples using XPS depth profiling measurements. The XPS depth profiling technique constantly etches the surface up to a certain depth using ion beams and acquire the composition. The XPS depth profiling results of bare Ni (111) foil, Ni (111) with 50 mg/ml, 100 mg/ml and 500 mg/ml spin coated phenolic resin is shown below.

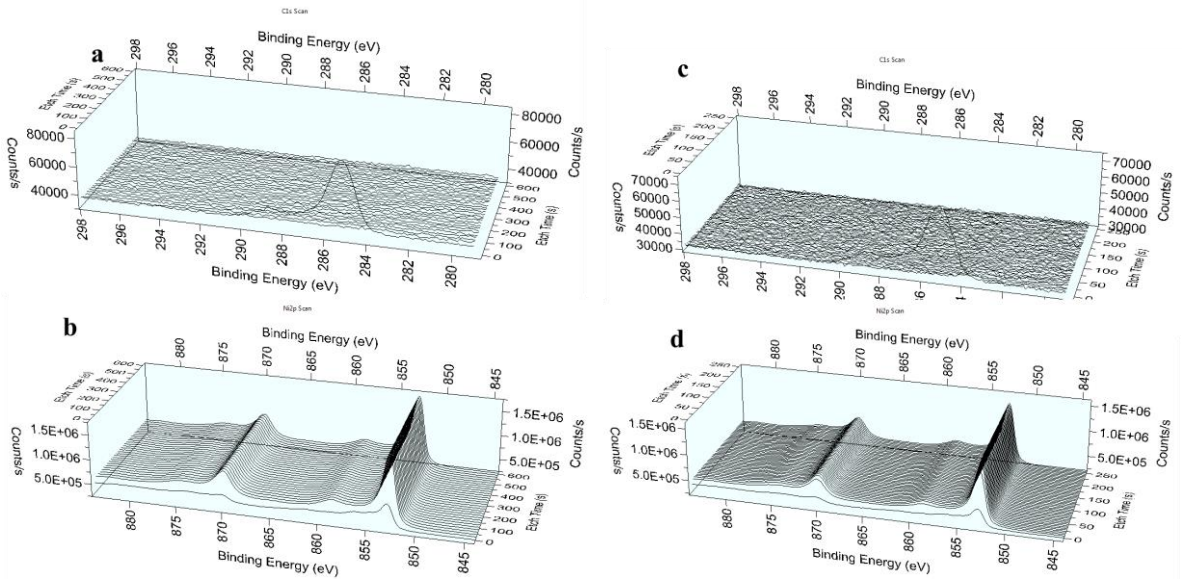

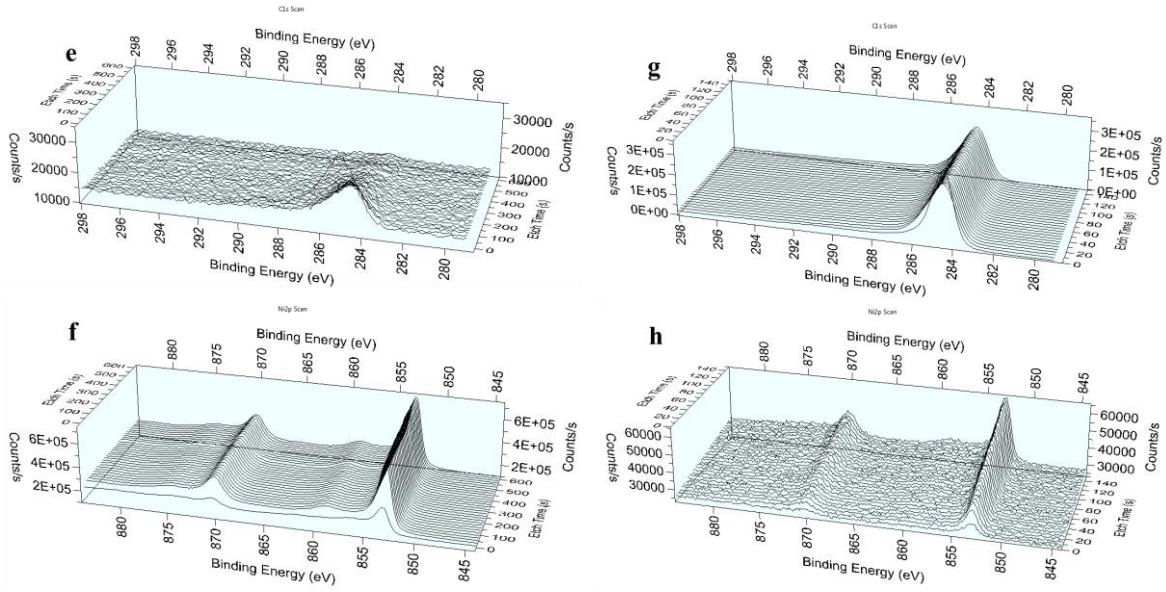

Figure 3.9: XPS depth profiling of phenolic resin coated Ni (111) after reaction; (a-b) C1s and Ni2p spectra of Bare Ni (111); C1s and Ni2p spectra of Ni (111)foil with 50 mg/ml (c-d) , 100 mg/ml (e-f) and 500 mg/ml (g-h) solution after annealing.

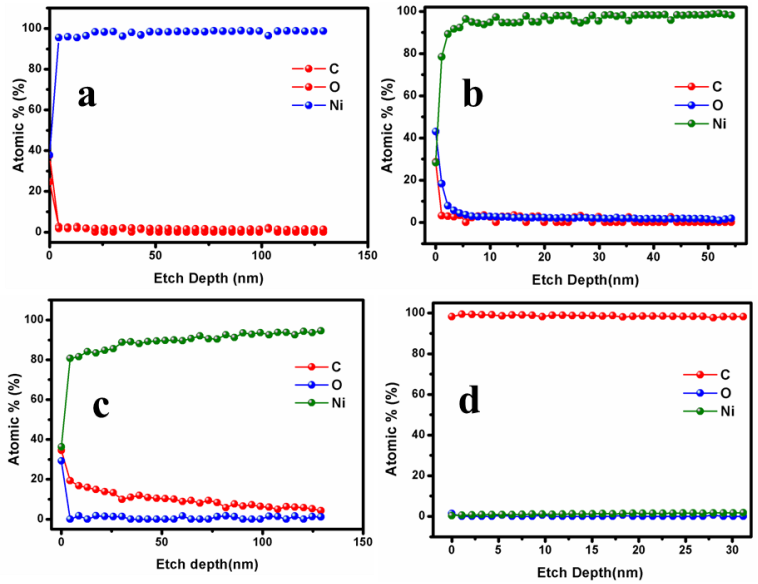

Figure 3.10: Atomic composition (C, Ni and O) at each etch cycle during XPS depth profiling; (a) bare Ni (111); (b) Ni (111) with 50 mg/ml Phenolic resin; (c) 100 mg/ml Phenolic resin; (d) 500 mg/ml Phenolic resin.

Figure 3.9 (a-h) show the XPS depth profiling results of all the aforementioned cases. For bare Ni (111), the C1s and Ni2p spectra collected after depth profiling is shown in

3.9(a-b). The C1s spectra showed a clear peak right before the etching is started. After the 1st etching, the C1s peak disappeared and up to a depth of ~100 nm, no signature of carbon was found. This clearly indicates that the C1s peak appeared before etching was due to some surface contamination, and is removed after the 1st etching cycle. The Ni2p spectra showed a much higher intense peak after the 1st etching cycle. The atomic composition (%) after each depth profiling cycle is collected and depicted in Figure 3.10(a-d) for all these mentioned cases. Figure 3.10 (a) clearly shows a sharp decrease in the carbon and oxygen concentration and an increase in the Ni concentration. This indicated the presence of carbon and oxygen on bare Ni (111), which mostly arises from the adsorbed species on the surface. Figure 3.9(c-d), (e-f) and (g-h) show the C1s and N1s spectra acquired for annealed samples of 50 mg/ml, 100 mg/ml and 500 mg/ml of phenolic resin. For 50 mg/ml case, behaviour similar to that of bare Ni (111) foil was observed, viz. no dissolved carbon was present. Hence, lack of sufficient concentration of phenolic resin is the reason for this observation. The atomic composition (%) of C and Ni also showed similar behaviour as that of bare Ni foil, shown in Figure 3.10(b). A different observation was seen after increasing the concentration to about 100 mg/ml. The C1s spectra accumulated at etch depth level showed a clear peak corresponding to C1s. However, we could not observe the presence of graphite or graphene in the whole area, rather some carbon patches were found. Apparently, the carbon that is decomposed from phenolic resin gets dissolved into the Ni (111) foil, which is not completely saturated and makes it to the surface via precipitation. The carbon composition after ~100 nm depth is ~5%, which is clear from Figure 3.10(c). By further increasing the phenolic resin concentration to about 500mg/ml, we could predominantly observe a thicker graphite film on the Ni (111) foil. The presence of large amount of carbon was confirmed through the depth profiling results. An etching up to 30 nm showed a very strong C1s peak, which confirms the large amount of carbon which is present. The AFM measurement confirmed that the graphite layer was more than 50 nm thick. The depth profiling data showed a very strong peak for C1s, which was from graphite. From figure 3.10(d), the carbon composition was ~100% up to 30 nm depth due to thicker layer of graphite. Therefore, to achieve thin-layer graphite on the metal surface with controlled layer numbers, further optimization by controlling the concentration of carbon species, cooling rate, heating time etc.., is necessary.

Along with conducting the growth on metal substrate, we did the same controlled experiment on quartz plate using the right concentration of carbon precursor and proper growth conditions followed for Ni foil. This was done for understanding the effect of the metal catalyst towards carbonization/graphitization.

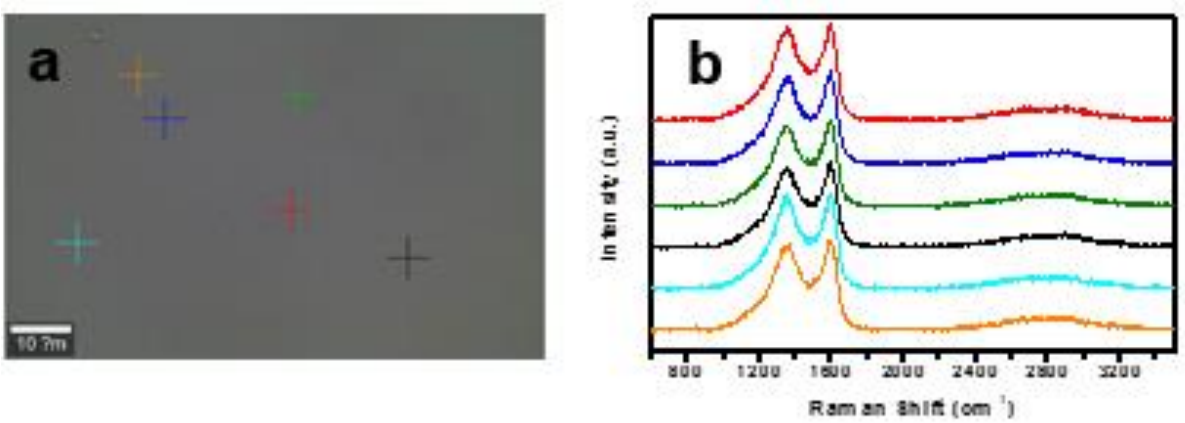

Figure 3.11: (a) & (b) Raman spectra of the carbon layer formed on quartz plate with phenolic resin solution.

Figure 3.11 (a) & (b) shows the Raman spectroscopy data collected from the carbon layer formed on the quartz plate at different locations. This data clearly suggested that the as formed black coloured substance was not graphite, rather it showed characteristics of amorphous type of carbon structure. This experiment helped us to understand the need of a metal catalyst to promote graphitization of carbon. Also, repeating the same experiment using lower concentrations of resin showed positive weight difference in the quartz plate. It thus gave a clue about the dissolved carbon in metal foil, Ni (111).

Besides transition metal assisted growth, we have also worked on thin-layer graphite/few layer graphene growth on Si/SiO_2 using micro mechanically exfoliated graphite as seed and phenolic resin as carbon source. The growth conditions were same as that of previously mentioned cases.

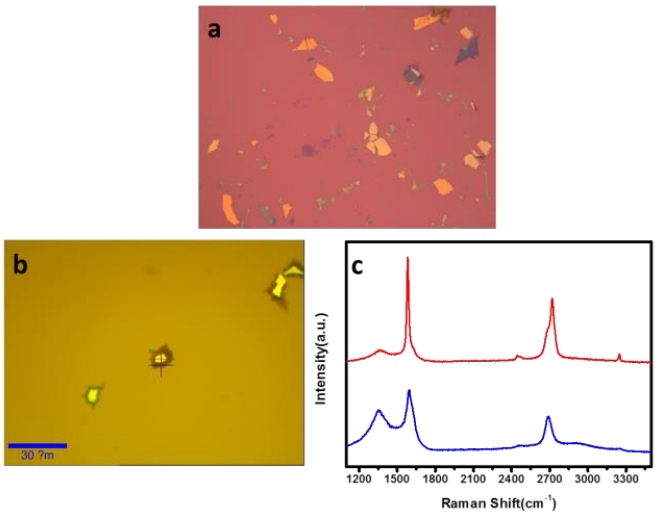

Figure 3.12: (a) Optical image of micromechanically exfoliated graphite sample with many graphite flakes, (b)Optical image of the substrate after annealing with phenolic resins, (c) Raman spectra of the same region.

Figure 3.12 (a) shows micromechanically exfoliated flakes of graphene from graphite on Si/SiO_2 under optical microscopy. Several graphene and graphite flakes can be seen vividly. Figure 3.12 (b) shows optical image of the same sample after heat treatment with phenolic resin. There appeared to be some additional graphene-like structure on every graphite flake which had started to grow. From Raman spectra (Figure 3.12 (c)), it was apparent that the central region was prominently graphite having sharp G peak and 2D peak. But the graphene-like structure grown around the graphite flakes was not clearly graphite. Nevertheless, it could be few layer graphene with many defects, because D band appeared larger in size. Hence, optimization is essential to obtain large area films with reduced defects by increasing the annealing time and concentration of phenolic resin.

3.2.2 Graphene growth on Cu and Cu-Ni foil by Chemical Vapour Deposition

Single-layer graphene was grown on polycrystalline Cu foil through chemical vapour deposition by using CH_4 as carbon source. The growth was performed at high temperature, 1050^oC, to achieve high quality graphene with no add layers. The mechanism of graphene growth on Cu is surface-catalysed and is self-limiting. That is once the Cu surface is covered with graphene, no further growth happens. Because of the low carbon solubility of Cu (less than 0.04 atomic %), it act as a good

substrate for monolayer graphene growth. However on Cu, it is difficult to get bilayer and multi-layer graphene. By modifying the growth techniques, people have successfully achieved bilayer graphene growth on copper substrate.[50] Nonetheless, as reported in most cases, it's really challenging to obtain high quality large area AB stacked bilayer graphene. However on Cu, addition of some high carbon-soluble metal like Ni can help forming Cu-Ni alloy which can then increase the carbon solubility of the substrate to get additional layers. From Cu-Ni phase diagram, it can be inferred that the alloy is stable and can be used for bilayer and multi-layer graphene growth. Cu-Ni alloy is commercially available with various compositions. Prof. R. S. Ruoff's group at UT Austin has achieved great success in growing high quality AB stacked bilayer and multi-layer graphene using commercially available Cu-Ni alloy (90/10 and 70/30 Cu/Ni).[32] They have also proved that the mechanism of graphene growth on Cu-Ni alloy is precipitation based and has shown by isotope labelling experiments using $^{12}CH_4$ and $^{13}CH_4$. However, it is challenging to achieve growth of large area continuous AB stacked bilayer graphene. In our project, we have used commercial Cu-Ni (90/10) alloy foil with a thickness of ~120 µm for bilayer graphene growth. The details regarding the growth conditions were explained in the experimental part. We performed growth of single-layer graphene on Cu foil and bilayer graphene growth on Cu-Ni (90/10) alloy.

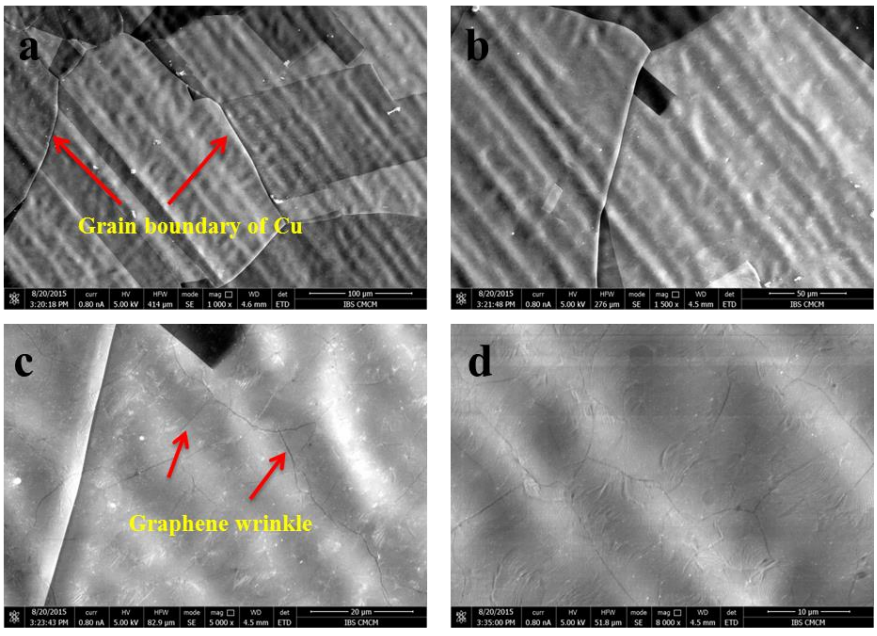

Figure 3.13: (a-d) SEM images of single-layer graphene on polycrystalline Cu foil.

Figure 3.13 (a-d) represents the SEM images of single-layer graphene on polycrystalline Cu foil at different magnifications. Cu grain boundaries can be seen from the low magnification images. The high magnification images shown in (c) and (d) illustrate obvious graphene wrinkles. From higher magnification images, it seems there are no additional layers present, which is an indication for a good quality single-layer graphene. Figure 3.14 depicts the Raman mapping data for single-layer graphene transferred to Si/SiO_2 substrate. Figure 3.14(a) shows the optical image of graphene on Si/SiO_2 and the red square represents the area (40 µm/40 µm) chosen for Raman mapping. Raman spectra collected after mapping is shown in Figure 3.14(b). The position for G band is at ~1580 cm^{-1} and the 2D band is at ~ 2675 cm^{-1}. These peaks are fingerprints of a typical single-layer graphene. The I_D/I_G ratio collected after mapping is shown in Figure 3.14(c). The presence of very negligible D band in the whole area confirms that the graphene is of high quality. The map for 2D FWHM is shown in Figure 3.14(d). In the whole mapping area, 2D FWHM is ~30-40 cm^{-1}, which is generally observed for single-layer graphene. All these data's clearly inferred the good quality nature of single-layer graphene.

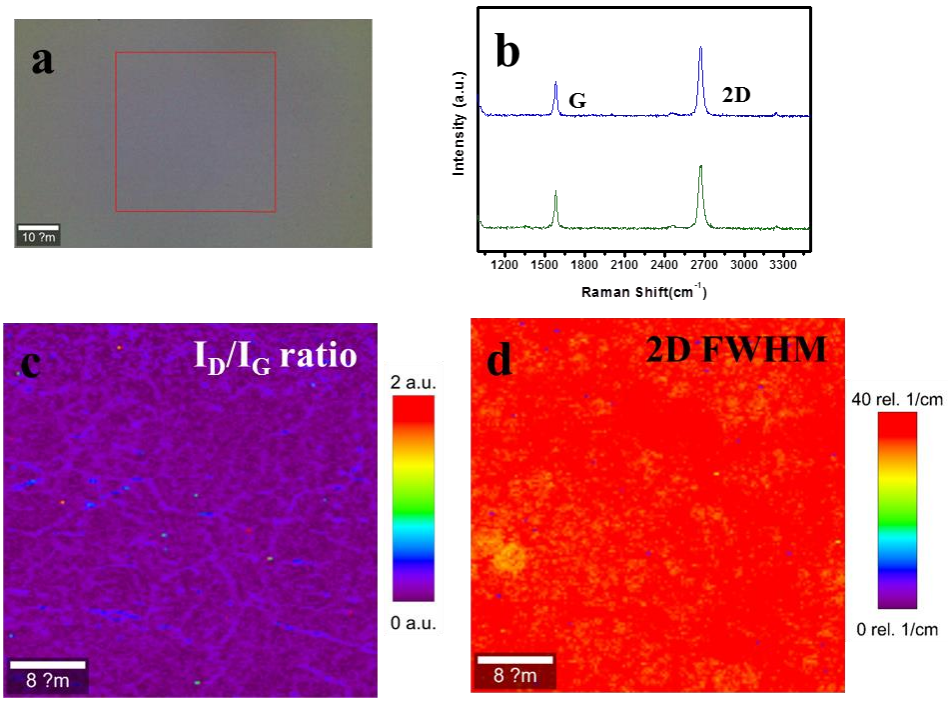

Figure 3.14: (a) Optical image of single-layer graphene transferred from Cu foil to Si/SiO_2, red square shows the area (40 µm/40 µm) chosen for Raman mapping; (b) Raman spectra collected from the mapping region; (c) I_D/I_G ratio calculated from Raman mapping; (d) Map of 2D FWHM.

Figure 3.15 shows the SEM images of as grown graphene on Cu-Ni (90/10) alloy. Figure 3.15 (a & b) shows the images of graphene with10 min growth time and Figure 3.15 (c &d) shows images of grown graphene when the growth time was 30 min. For 10 min growth time, the foil is covered with single-layer graphene along with few bilayer patches. Both single and bilayer regions were identified with Raman spectra, shown in Figure 3.16. Raman spectra corroborated that the bilayer patches formed were AB stacked. Then the growth time was increased to 30 min, aimed at growing continuous bilayer film from bilayer islands. The SEM images showed no contrast difference, confirmed the formation of a continuous film. The sample was then transferred to Si/SiO_2 for Raman analysis.

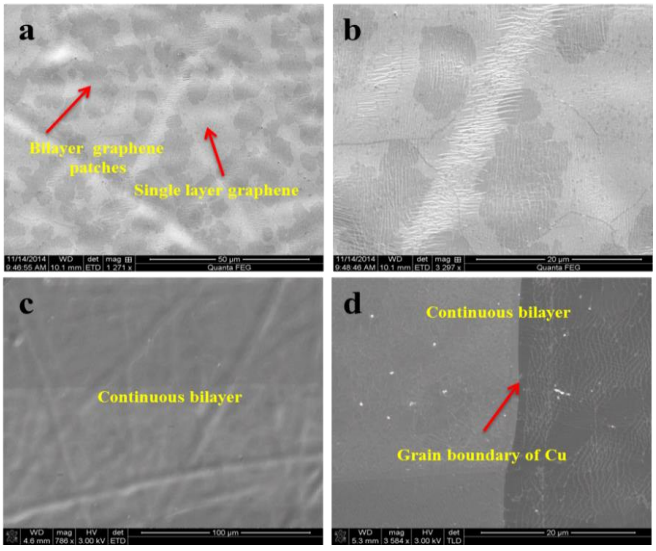

Figure 3.15: SEM images of bilayer graphene grown on commercial Cu-Ni alloy foil; (a-b) SEM images of bilayer islands; (c-d) SEM images of continuous bilayer film on Cu-Ni foil.

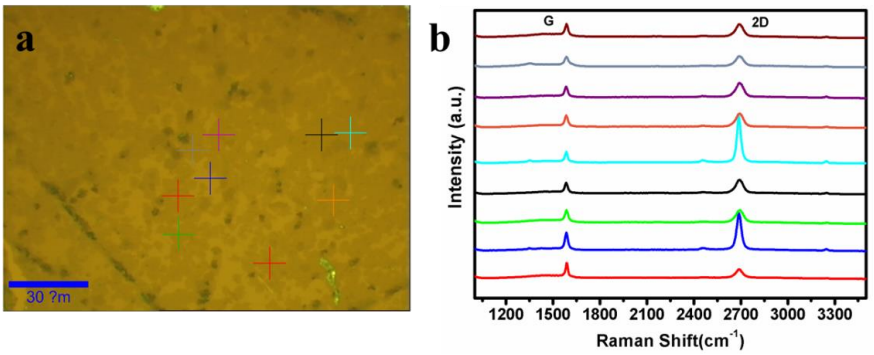

Figure 3.16: (a) Optical image of bilayer graphene grown on Cu-Ni (90/10) alloy transferred to a Si/SiO_2 substrate, (b) Raman spectra of the same region at different positions.

The Raman mapping data for the continuous bilayer graphene sample is shown in Figure 3.17. The optical image of the transferred bilayer graphene is shown in Figure 3.17(a). The image clearly shows the presence of continuous bilayer region along with fewer regions having single and multi-layer portions. The Raman spectra collected from the mapping region (30 µm/30 µm area) is shown in Figure 3.17(b). The spectra is collected from regions where both AB stacked and mis-oriented (not AB stacked) bilayer graphene is present. The I_G/I_{2D} ratio of the given AB stacked bilayer graphene is ~0.7-1.2 and 2D peak has an obvious shoulder peak.

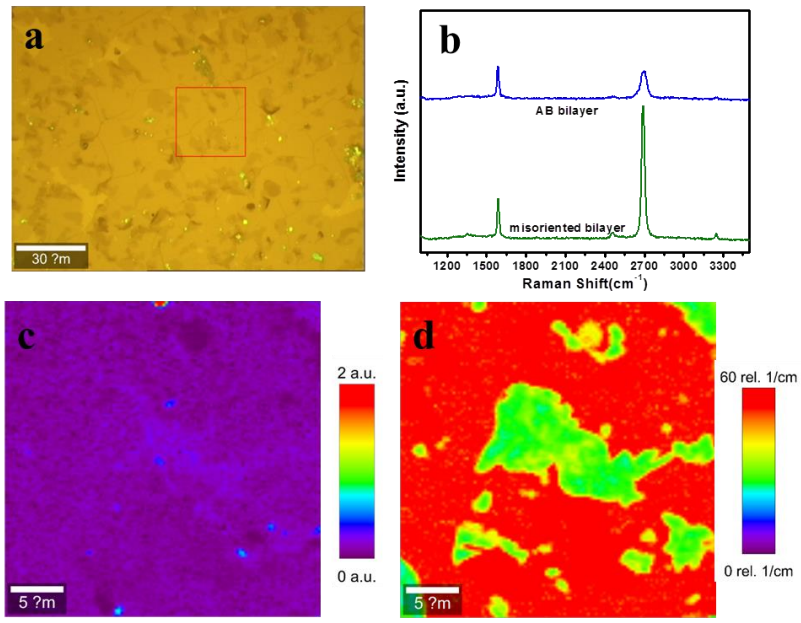

Figure 3.17: (a) Optical image of single-layer graphene transferred from Cu-Ni foil to Si/SiO_2, red square shows Raman mapping area (30 µm/30 µm); (b) Raman spectra collected from the mapping region;(c) I_D/I_G ratio calculated from Raman mapping; (d) Map for 2D FWHM.

In non-AB stacked bilayer graphene, both the layers behave as individual single-layer graphene and the Raman spectra shows characteristics of a single-layer graphene, and that is what is shown in Figure 3.17(b). The miss-oriented bilayer graphene is commonly seen at some places during the growth. Figure 3.17 (c & d) shows maps for I_D/I_G ratio and 2D FWHM. The I_D/I_G ratio showed negligible D band, indicating good quality of graphene. A 2D FWHM value of ~55-60 cm^{-1} was observed in most of the regions, which is typical for AB stacked bilayer graphene. At some places, the green-coloured region showed the lower 2D FWHM value (~30-40 cm^{-1}), corresponds to disoriented bilayer graphene. These data's clearly says that further optimization is essential to achieve the growth of large area AB stacked bilayer graphene.

Conclusion

In this work, we investigated the growth of large area graphene and thin-layer graphite on various substrates, primarily by utilizing the catalytic effect of transition metals.

With the help of chemical vapour deposition (CVD) and carbon source as hydrocarbon gas molecule, we successfully achieved the growth of high quality monolayer graphene on Cu and AB stacked bilayer graphene on Cu-Ni alloy. However, a lot of progress need to be done for high quality large area bilayer graphene with minimal multi-layer coverage.

We succeeded in synthesising thin-layer graphite (few layer graphene) on polycrystalline Ni foil and using phenolic resin as carbon source. Homemade mono crystalline Ni (111) catalyst showed interesting results. However, control over graphene layer number in graphite is still remain as a major constraint. For that, optimizing growth conditions are currently underway.

Our efforts with growing graphene/thin-layer graphite on metal and dielectric substrate (Si/SiO_2) using mechanically exfoliated graphite as a seed and amorphous carbon source has also showed progress up to certain extend. However, further optimization in the growth conditions are yet to be done.

Bibliography

1. Zhu, Y. W.; Murali, S.; Cai, W. W.; Li, X. S.; Suk, J. W.; Potts, J. R.; Ruoff, R. S., Graphene and Graphene Oxide: Synthesis, Properties, and Applications. *Advanced Materials* **2010,** *22* (35), 3906-3924.
2. Wallace, P. R., Erratum: The Band Theory of Graphite [Phys. Rev. 71, 622 (1947)]. *Physical Review* **1947,** *72* (3), 258-258.
3. Dreyer, D. R.; Ruoff, R. S.; Bielawski, C. W., From Conception to Realization: An Historial Account of Graphene and Some Perspectives for Its Future. *Angewandte Chemie-International Edition* **2010,** *49* (49), 9336-9344.
4. Frohs, W.; von Sturm, F.; Wege, E.; Nutsch, G.; Handl, W., Carbon, 3. Graphite. In *Ullmann's Encyclopedia of Industrial Chemistry*, Wiley-VCH Verlag GmbH & Co. KGaA: 2000.
5. Geim, A. K.; Novoselov, K. S., The rise of graphene. *Nature Materials* **2007,** *6* (3), 183-191.
6. Stankovich, S.; Dikin, D. A.; Dommett, G. H. B.; Kohlhaas, K. M.; Zimney, E. J.; Stach, E. A.; Piner, R. D.; Nguyen, S. T.; Ruoff, R. S., Graphene-based composite materials. *Nature* **2006,** *442* (7100), 282-286.
7. Stankovich, S.; Dikin, D. A.; Piner, R. D.; Kohlhaas, K. A.; Kleinhammes, A.; Jia, Y.; Wu, Y.; Nguyen, S. T.; Ruoff, R. S., Synthesis of graphene-based nanosheets via chemical reduction of exfoliated graphite oxide. *Carbon* **2007,** *45* (7), 1558-1565.
8. Zhu, Y. W.; Stoller, M. D.; Cai, W. W.; Velamakanni, A.; Piner, R. D.; Chen, D.; Ruoff, R. S., Exfoliation of Graphite Oxide in Propylene Carbonate and Thermal Reduction of the Resulting Graphene Oxide Platelets. *Acs Nano* **2010,** *4* (2), 1227-1233.
9. Robinson, J.; Weng, X.; Trumbull, K.; Cavalero, R.; Wetherington, M.; Frantz, E.; LaBella, M.; Hughes, Z.; Fanton, M.; Snyder, D., Nucleation of Epitaxial Graphene on SiC(0001). *ACS Nano* **2010,** *4* (1), 153-158.
10. Li, X. S.; Cai, W. W.; An, J. H.; Kim, S.; Nah, J.; Yang, D. X.; Piner, R.; Velamakanni, A.; Jung, I.; Tutuc, E.; Banerjee, S. K.; Colombo, L.; Ruoff, R. S., Large-Area Synthesis of High-Quality and Uniform Graphene Films on Copper Foils. *Science* **2009,** *324* (5932), 1312-1314.
11. Wang, C.; Chen, W.; Han, C.; Wang, G.; Tang, B.; Tang, C.; Wang, Y.; Zou, W.; Chen, W.; Zhang, X.-A.; Qin, S.; Chang, S.; Wang, L., Growth of Millimeter-Size Single Crystal Graphene on Cu Foils by Circumfluence Chemical Vapor Deposition. *Scientific Reports* **2014,** *4*, 4537.
12. Muñoz, R.; Gómez-Aleixandre, C., Review of CVD Synthesis of Graphene. *Chemical Vapor Deposition* **2013,** *19* (10-11-12), 297-322.
13. Noda, T.; Inagaki, M., Effect of gas phase on graphitization of carbon. *Carbon* **1964,** *2* (2), 127-130.
14. Shelton, J. C.; Patil, H. R.; Blakely, J. M., Equilibrium Segregation of Carbon to a Nickel (111) Surface - Surface Phase-Transition. *Surface Science* **1974,** *43* (2), 493-520.
15. Li, X. S.; Cai, W. W.; Colombo, L.; Ruoff, R. S., Evolution of Graphene Growth on Ni and Cu by Carbon Isotope Labeling. *Nano Letters* **2009,** *9* (12), 4268-4272.
16. Eizenberg, M.; Blakely, J. M., Carbon Monolayer Phase Condensation on Ni(111). *Surface Science* **1979,** *82* (1), 228-236.
17. Dahal, A.; Batzill, M., Graphene-nickel interfaces: a review. *Nanoscale* **2014,** *6* (5), 2548-2562.

18. Robertso.Sd, Graphite Formation from Low Temperature Pyrolysis of Methane over Some Transition Metal Surfaces. *Nature* **1969,** *221* (5185), 1044-&.
19. Cai, W. W.; Piner, R. D.; Zhu, Y. W.; Li, X. S.; Tan, Z. B.; Floresca, H. C.; Yang, C. L.; Lu, L.; Kim, M. J.; Ruoff, R. S., Synthesis of Isotopically-Labeled Graphite Films by Cold-Wall Chemical Vapor Deposition and Electronic Properties of Graphene Obtained from Such Films. *Nano Research* **2009,** *2* (11), 851-856.
20. Li, X. S.; Magnuson, C. W.; Venugopal, A.; Tromp, R. M.; Hannon, J. B.; Vogel, E. M.; Colombo, L.; Ruoff, R. S., Large-Area Graphene Single Crystals Grown by Low-Pressure Chemical Vapor Deposition of Methane on Copper. *Journal of the American Chemical Society* **2011,** *133* (9), 2816-2819.
21. Chen, S. S.; Cai, W. W.; Piner, R. D.; Suk, J. W.; Wu, Y. P.; Ren, Y. J.; Kang, J. Y.; Ruoff, R. S., Synthesis and Characterization of Large-Area Graphene and Graphite Films on Commercial Cu-Ni Alloy Foils. *Nano Letters* **2011,** *11* (9), 3519-3525.
22. Zhang, Y.; Zhang, L.; Zhou, C., Review of Chemical Vapor Deposition of Graphene and Related Applications. *Accounts of Chemical Research* **2013,** *46* (10), 2329-2339.
23. McLellan, R. B., The solubility of carbon in solid gold, copper, and silver. *Scripta Metallurgica* **1969,** *3* (6), 389-391.
24. López, G. A.; Mittemeijer, E. J., The solubility of C in solid Cu. *Scripta Materialia* **2004,** *51* (1), 1-5.
25. Mathieu, G.; Guiot, S.; Cabané, J., Solubilite du carbone dans l'argent, le cuivre et l'or. *Scripta Metallurgica* **1973,** *7* (4), 421-425.
26. Seah, C.-M.; Chai, S.-P.; Mohamed, A. R., Mechanisms of graphene growth by chemical vapour deposition on transition metals. *Carbon* **2014,** *70*, 1-21.
27. Ravi Kumar, N. V.; Mager, R.; Cai, Y.; Zimmermann, A.; Aldinger, F., High temperature deformation behaviour of crystallized Si–B–C–N ceramics obtained from a boron modified poly(vinyl)silazane polymeric precursor. *Scripta Materialia* **2004,** *51* (1), 65-69.
28. Chen, S.; Cai, W.; Piner, R. D.; Suk, J. W.; Wu, Y.; Ren, Y.; Kang, J.; Ruoff, R. S., Synthesis and Characterization of Large-Area Graphene and Graphite Films on Commercial Cu–Ni Alloy Foils. *Nano Letters* **2011,** *11* (9), 3519-3525.
29. Wu, Y.; Chou, H.; Ji, H.; Wu, Q.; Chen, S.; Jiang, W.; Hao, Y.; Kang, J.; Ren, Y.; Piner, R. D.; Ruoff, R. S., Growth Mechanism and Controlled Synthesis of AB-Stacked Bilayer Graphene on Cu–Ni Alloy Foils. *ACS Nano* **2012,** *6* (9), 7731-7738.
30. Sun, H.-B.; Wu, J.; Han, Y.; Wang, J.-Y.; Song, F.-Q.; Wan, J.-G., Nonisothermal Synthesis of AB-Stacked Bilayer Graphene on Cu Foils by Atmospheric Pressure Chemical Vapor Deposition. *The Journal of Physical Chemistry C* **2014,** *118* (26), 14655-14661.
31. Fang, W.; Hsu, A. L.; Song, Y.; Birdwell, A. G.; Amani, M.; Dubey, M.; Dresselhaus, M. S.; Palacios, T.; Kong, J., Asymmetric Growth of Bilayer Graphene on Copper Enclosures Using Low-Pressure Chemical Vapor Deposition. *ACS Nano* **2014,** *8* (6), 6491-6499.
32. Wu, Y. P.; Chou, H.; Ji, H. X.; Wu, Q. Z.; Chen, S. S.; Jiang, W.; Hao, Y. F.; Kang, J. Y.; Ren, Y. J.; Piner, R. D.; Ruoff, R. S., Growth Mechanism and Controlled Synthesis of AB-Stacked Bilayer Graphene on Cu-Ni Alloy Foils. *Acs Nano* **2012,** *6* (9), 7731-7738.
33. Zhang, Y.; Gomez, L.; Ishikawa, F. N.; Madaria, A.; Ryu, K.; Wang, C.; Badmaev, A.; Zhou, C., Comparison of Graphene Growth on Single-Crystalline and Polycrystalline Ni by Chemical Vapor Deposition. *The Journal of Physical Chemistry Letters* **2010,** *1* (20), 3101-3107.
34. Addou, R.; Dahal, A.; Sutter, P.; Batzill, M., Monolayer graphene growth on Ni(111) by low temperature chemical vapor deposition. *Applied Physics Letters* **2012,** *100* (2), 021601.
35. Isett, L. C.; Blakely, J. M., Segregation Isosteres for Carbon at (100) Surface of Nickel. *Surface Science* **1976,** *58* (2), 397-414.

36. Eizenberg, M.; Blakely, J. M., Carbon Interaction with Nickel Surfaces - Monolayer Formation and Structural Stability. *Journal of Chemical Physics* **1979,** *71* (8), 3467-3477.
37. Zhang, Y.; Gomez, L.; Ishikawa, F. N.; Madaria, A.; Ryu, K.; Wang, C. A.; Badmaev, A.; Zhou, C. W., Comparison of Graphene Growth on Single-Crystalline and Polycrystalline Ni by Chemical Vapor Deposition. *Journal of Physical Chemistry Letters* **2010,** *1* (20), 3101-3107.
38. Patil, H. R.; Blakely, J. M., Electron energy losses in thin graphite layers on the (111) face of nickel. *Journal of Applied Physics* **1974,** *45* (9), 3806-3808.
39. Yamazaki, S.; Tanaka, M.; Tanaka, S.; Fuginami, M.; Uemori, R.; Fujita, D.; Homma, T.; Ono, M., Atomic Images and Defect Structures of the Epitaxially Precipitated Carbon Layers on Ni(111) Surface. *Journal of Vacuum Science & Technology B* **1991,** *9* (2), 883-885.
40. Kim, K. S.; Zhao, Y.; Jang, H.; Lee, S. Y.; Kim, J. M.; Kim, K. S.; Ahn, J.-H.; Kim, P.; Choi, J.-Y.; Hong, B. H., Large-scale pattern growth of graphene films for stretchable transparent electrodes. *Nature* **2009,** *457* (7230), 706-710.
41. Sun, Z.; Yan, Z.; Yao, J.; Beitler, E.; Zhu, Y.; Tour, J. M., Growth of graphene from solid carbon sources. *Nature* **2010,** *468* (7323), 549-552.
42. Wewerka, E. M., The determination of the molecular distributions of graphite binder materials by gel permeation chromatography. *Carbon* **1968,** *6* (1), 93-100.
43. Yamashita, Y.; Ouchi, K., A Study on Carbonization of Phenol-Formaldehyde Resin Labeled with Deuterium and C-13. *Carbon* **1981,** *19* (2), 89-94.
44. Zhao, M.; Song, H. H., Catalytic Graphitization of Phenolic Resin. *Journal of Materials Science & Technology* **2011,** *27* (3), 266-270.
45. Shun'ko, E. V., I-V characteristics of the Langmuir probe in flowing afterglow plasmas. *Journal of Applied Physics* **2003,** *93* (7), 3729-3746.
46. Li, X. S.; Zhu, Y. W.; Cai, W. W.; Borysiak, M.; Han, B. Y.; Chen, D.; Piner, R. D.; Colombo, L.; Ruoff, R. S., Transfer of Large-Area Graphene Films for High-Performance Transparent Conductive Electrodes. *Nano Letters* **2009,** *9* (12), 4359-4363.
47. Gao, L. B.; Ren, W. C.; Xu, H. L.; Jin, L.; Wang, Z. X.; Ma, T.; Ma, L. P.; Zhang, Z. Y.; Fu, Q.; Peng, L. M.; Bao, X. H.; Cheng, H. M., Repeated growth and bubbling transfer of graphene with millimetre-size single-crystal grains using platinum. *Nature Communications* **2012,** *3*.
48. Ferrari, A. C.; Meyer, J. C.; Scardaci, V.; Casiraghi, C.; Lazzeri, M.; Mauri, F.; Piscanec, S.; Jiang, D.; Novoselov, K. S.; Roth, S.; Geim, A. K., Raman spectrum of graphene and graphene layers. *Physical Review Letters* **2006,** *97* (18).
49. Yudasaka, M.; Kikuchi, R.; Ohki, Y.; Yoshimura, S., Graphite growth influenced by crystallographic faces of Ni films. *Journal of Vacuum Science & Technology A* **1998,** *16* (4), 2463-2465.
50. Fang, W.; Hsu, A. L.; Caudillo, R.; Song, Y.; Birdwell, A. G.; Zakar, E.; Kalbac, M.; Dubey, M.; Palacios, T.; Dresselhaus, M. S.; Araujo, P. T.; Kong, J., Rapid Identification of Stacking Orientation in Isotopically Labeled Chemical-Vapor Grown Bilayer Graphene by Raman Spectroscopy. *Nano Letters* **2013,** *13* (4), 1541-1548.